**ETH Institute for
Particle Physics**

DIPLOMA THESIS

Topological Reconstruction of Decays with Missing Particles

Daniel Wiesmann
under the supervision of
Prof. Dr. Urs Langenegger

ETH Zürich, Switzerland

Abstract

Three reconstruction methods have been developed. The methods can be applied to reconstruct events with missing particles using topological information. An analysis of the two decays $B_s^0 \rightarrow \tau^+\tau^-$ and $B_s^0 \rightarrow \mu^\pm\tau^\mp$ has been performed on simulated data using the presented methods. It has been shown that in a realistic experimental environment a mass resolution of 900 MeV should be achievable in the reconstruction of the decay $B_s^0 \rightarrow \tau^+\tau^-$. Similarly the expected mass resolution in the reconstruction of the decay $B_s^0 \rightarrow \mu^\pm\tau^\mp$ is 700 MeV. In principle both decays can now be studied with the presented reconstruction methods and it should be possible to put upper bounds on their branching ratios in experiments.

Contents

Chapter 0

Introduction

Advanced particle physics experiments as they are done in our time have almost
nothing to do anymore with the classical picture one has of a physics experiment.
What today is referred to as measurement in particle physics is an analysis of
data sets which where taken at machines that can never be built and even hardly
overviewed by only one person. The outcome of any measurement with such a
machine relies on the effort of many people. In this thesis three analysis methods
shall be presented which can be used to make measurements in the sense described
above. It is clear that an analysis method is only one of the many contributions
which are necessary to make final results possible. Any method is worthless without
real experiments which allow its application. Still the introduction of an analysis
method should not depend on the concrete experimental set up. It is developed to
test physical laws and therefore it should be applicable in different experimental en-
vironments. Of course the results obtained with the analysis method should be the
same at different experiments. An analysis must also have a theoretical motivation
and the physical laws which can be tested with such a method should be declared.
The organization of this thesis is chosen such that the considerations above are re-
spected as well as possible. In Chapter 1 an experiment is described which should
allow the application of the presented reconstruction methods. Chapter 2 gives a
theoretical motivation for the analysis methods. The methods are then formally
introduced in Chapter 3, where no assumption about a concrete experimental set
up is made. Finally in Chapter 4 the methods are applied to simulated data and a
complete analysis is performed in order to show what could be the outcome of such
an analysis on real data.

The methods provide a possibility to reconstruct decays containing missing parti-
cles. Such decays are difficult to reconstruct because the missing particles carry
away information about the initial energy and momentum contained in the decay.
It will be shown that the reconstruction of the decays can anyhow be done by using
topological information. The possibility to reconstruct two sorts of decays with two
different decay topologies will be developed. A concrete analysis will be performed

on the following simulated decays:

$$B_s^0 \to \tau^+\tau^- \quad \text{and} \quad B_s^0 \to \mu^\pm\tau^\mp.$$

These decays are excellent examples for the decay topologies which are studied here.

Chapter 1

Experimental Environment

1.1   The Large Hadron Collider

The Large Hadron Collider (LHC) is a particle accelerator which is currently under construction at the European Organization for Nuclear Research (CERN) near Geneva, Switzerland. Once the construction of the LHC is finished, it will be the worlds largest particle accelerator capable to accelerate hadrons to energies never reached before in accelerator experiments. According to the official schedule, the accelerator will be ready for first test runs in November 2007. The maximal center of mass energy for proton-proton collisions will be $\sqrt{s} = 14$ TeV and is expected to be obtained after commissioning in the beginning of 2008. However since the proton is not an elementary particle, at these high energies the relevant physical quantity for the scattering process is not the center of mass energy of the protons but rather the resulting center of mass energies for collisions of the quarks in the proton. The quarks of a proton carry roughly 1/6 of its total energy and so for a collision between two quarks the energy will be $\sqrt{s} = 14 \cdot 1/6 \sim 2$ TeV. This is still an energy that has not yet been reached in experiments with collisions between elementary particles and so the discovery of new physics is expected at the LHC. It will also be possible to accelerate lead nuclei, such that in collisions center of mass energies of about 1150 TeV will be reached. This will provide new insights into the detailed properties of quark-gluon plasma.

To achieve those very high center of mass energies, there is a whole system of smaller particle accelerators which successively raise the particle energies before they are actually injected into the LHC. The LHC is the last link in this chain and for instance the energy of the protons before injection will already amount 450 GeV. A schematic view on the different stages of accelerators and the detectors at CERN is given in Figure 1.1.

There are six detectors which are going to do experiments using the high energetic particles from the LHC. Their acronyms are CMS, ATLAS, LHCb, ALICE, TOTEM, and LHCf. The two experiments CMS (Compact Muon Solenoid) and ATLAS (A Toroidal LHC AparatuS) have rather general designs in order to be pre-
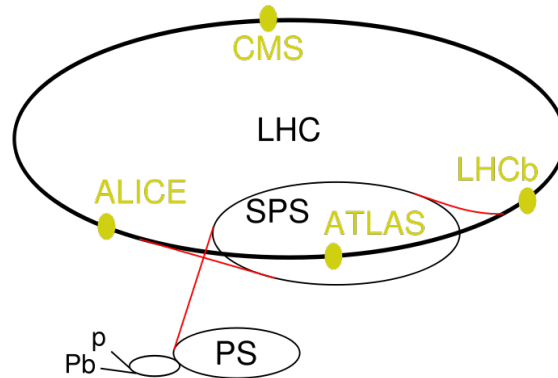
7

Figure 1.1: The LHC accelerator chain and experiments.

pared as well as possible for all kinds of new physics. The other four experiments are more specialized on specific topics of interest in particle physics. So if there are any breakthrough discoveries to make with the new accelerator, they are expected do be made at CMS and ATLAS. There are five experiments located at the interaction region. Four of those experiments are displayed in Figure 1.1, the TOTEM experiment is not displayed explicitly, but shares an interaction point with the CMS experiment.

1.2   The CMS Experiment

Any measurement and analysis method based on physical concepts must be general in the sense that it should not depend on its concrete realization. The concepts it contains must be formulated in such a way that they can be applied within different experimental environments. So throughout this work three analysis methods will be presented independently of a specific framework. But in order to show its validity, the analysis procedure must then also be applied to an experiment. So a specific experimental setup which allows such a verification must be declared. The setup concerning this work is the CMS experiment at the LHC, and thus a brief description of this experiment is given. At this point it is important to stress again that the constructions of LHC and also of the CMS experiment are not yet finished and so no data at all has been taken so far. The verification of the presented analysis procedures will only be made on simulated data. A possible final test to the methods can only be done later on when the LHC will be running or maybe also at other collider experiments.

In principle the design of the CMS experiment is similar to most standard particle detectors existing today. The experiment is displayed in Figure 1.2. There is a barrel pixel detector with 48 million pixels for vertexing in the innermost of the detector.
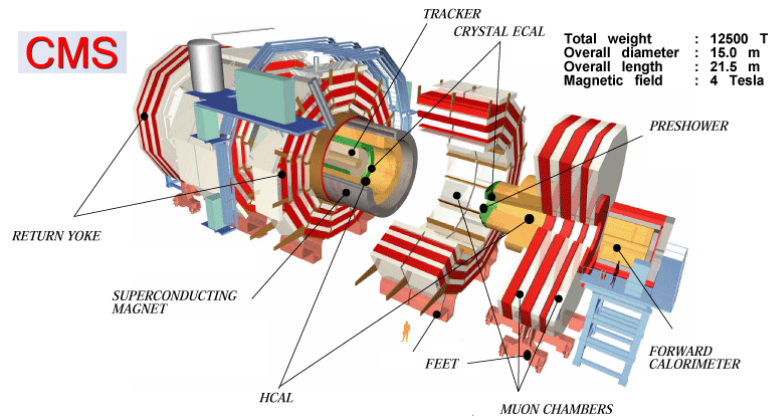
Figure 1.2: The CMS Experiment.

The pixel detector is surrounded by a silicon strip tracking system and a crystal electromagnetic calorimeter. After the electromagnetic calorimeter the hadronic calorimeter is placed. All these four different subdetectors are located within a very strong solenoid magnet with a field strength of 4 Tesla. Since the costs of such a strong magnet rise rapidly with its size, the whole setup including the magnet is built relatively compact in order to be able to build up a such strong magnetic field in the area with these four first subdetectors. The error on the momentum measurements depends linearly on the magnetic field within the tracking system and quadratically on the length of the measured track. So in the design of a detector like CMS, an optimal balance between size and field strength obtainable with a given budget had to be found. The last subdetector is a muon system placed around the solenoid magnet. The muon chambers are mounted between the big iron return yoke of the magnet.

1.3 Physics at the LHC

Two detectors at LHC, namely the CMS and the ATLAS experiments, have to be singled out because, within the six experiments under construction, those two are the most likely to discover new physics. Most particle physicists today believe that the discovery of the theoretically predicted Higgs boson will be made within the first few years of data taking at CMS and ATLAS. Since the shut down of LEP in 2000, the construction of the LHC has begun and it will only be finished towards the end of this year. During the period in between there have been only a few other colliders that have reached energy scales which where substantially higher than the scale at which LEP was running. None of these other colliders run at energies comparable to what the LHC can reach. So there has been a long waiting time for new data.

Due to the scale dependence of modern field theories it is possible to invent new theories which only show deviations from the Standard Model (SM) at energies not obtained so far and thus are consistent with present observations. This gave rise to a broad variety of theoretical models predicting all kinds of new phenomena which possibly could be seen at the high energy scales reached by the LHC in the near future. Examples for the new phenomena are theories with new particles and symmetries [11], extra dimensions [12], explanations for dark matter [13] and also other properties [14]. The spectrum of different models today can hardly be overviewed, but still in principle all models that do coincide with current data should be taken seriously and compared with experiments as much as possible. The future measurements at the LHC are hopefully going to shed some light on this variety of theoretical models by ruling out some of them or, thinking more optimistically, even by finding evidence for them. It has been shown theoretically that for some of the most promising and popular models beyond the standard model, the LHC will be able to either confirm or exclude those models within the whole range of interest in their parameter space.

Chapter 2

Theoretical Motivation

In this work three different reconstruction methods will be presented. All three methods provide a possibility to reconstruct rare leptonic B_s^0 meson decays. The two decays that are going to be studied here are

$$B_s^0 \to \tau^+\tau^- \quad \text{and} \quad B_s^0 \to \mu^\pm\tau^\mp.$$

The Feynmann diagrams for both decays are displayed in Figure 2.1. To date neither of the two decays have been observed or given upper bounds on the branching ratio. The measurement of such decays is difficult because these are rare B decays. In the Standard Model (SM) the decays $B \to l^+l^-$ are helicity suppressed by a factor of $(m_l/m_B)^2$. The theoretical predictions for the branching ratios of such decays are very precise and still at least two orders of magnitude smaller than the present experimental upper bounds. In models beyond the SM these branching ratios can be enhanced by orders of magnitude due to additional mediating particles in the loop- and box diagrams for these processes. This additional mediating particles are symbolically indicated by X in Figure 2.1. Since the upper bounds are not yet on the level of the SM predictions, there is still a possibility to detect deviations from the SM by measuring the branching ratios of rare B decays. So in the last few years there has been increasing interest in rare leptonic B decays ([1], [2], [3], [4]). Future analyses on these quantities will provide strong restrictions not only on the measured quantities themselves, but also on the possible parameter space of models that go beyond the standard model. Theorists have put special emphasis on supersymmetric extensions of the SM, such as the Minimal Supersymmetric Standard Model (MSSM) or Two-Higgs Doublet Models (2HDM). The branching ratios of the decays grow as $\tan^6\beta$ in the MSSM and as $\tan^4\beta$ in the 2HDM. On a theoretical level these models are understood quite well and the branching fractions for many different sets of parameters have been computed. The LHC will run at energies where many of the new models can be seriously tested.

Due to the mass dependent suppression factor, the measurement of a B meson decaying into electrons is out of reach for present day experiments and also for the future measurements at the LHC. The decay into muons provides a clear experimental signature and is not so strongly suppressed as the electron channel. So it has
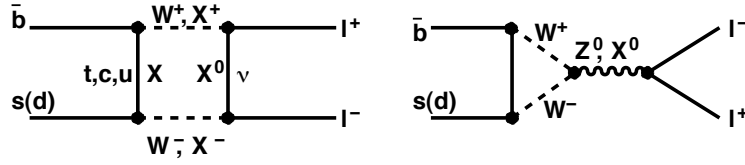
Figure 2.1: The box (left) and loop (right) interactions in the decay $B_s^0 \to \tau\tau$ and $B_s^0 \to \mu\tau$. In the SM the interactions are mediated via $W^{\pm}$ and Z^0 bosons. In some SM extensions these decays can also be mediated by other new particles leading to an enhancement of the branching fraction. The new particles are symbolically denoted with X.

been tested at CDF [2] and the best experimental upper bounds for the branching ratios are $\mathcal{B}(B_s^0 \to \mu^+\mu^-) < 1.5 \times 10^{-7}$ and $\mathcal{B}(B_d^0 \to \mu^+\mu^-) < 3.9 \times 10^{-8}$ at the 90% C.L. The decay of a B_s^0 into τ-leptons which will be presented here is interesting because it is the least suppressed channel due to the large τ mass. The disadvantage is, that this decay has a difficult experimental signature because at least two neutrinos appear within the decay. The theoretical prediction for this branching ratio in the SM is ([8], [9])

$$\mathcal{B}(B_s^0 \to \tau^+\tau^-)^{SM} = (7.31 \pm 1.1) \times 10^{-7}.$$

For the lepton flavor violating decay $B_s^0 \to \mu\tau$ the suppression is extremely high because it depends on neutrino oscillations. The neutrino mediating between the μ-lepton and the τ-lepton must change flavor within the process and this is very unlikely to happen in the SM. So the resulting theoretical branching ratio can be regarded as ~ 0 in the SM. The decay mode has been studied experimentally for the lighter B_d^0 meson in [5]. An example where a neutral Higgs boson could enhance the decay for the B_s^0 meson is discussed in [6].

Chapter 3

Formal Reconstruction

This chapter presents three analysis methods on a formal level. The methods can be used for the reconstruction of short cascades of two-body decays. The reconstruction will be done using topological information. It has been shown in [7] that topological information can be a powerful tool to reconstruct decays with missing energy and momentum. Particles that can not be detected in an experiment carry away an unknown amount of energy and momentum. This makes the reconstruction of a decay containing missing particles difficult. The presented methods will provide a possibility to reconstruct such decays, despite the lack of information in the decay. Two applications have been chosen, both are good examples to illustrate the possibilities of the methods. The main focus was laid on the decay $B_s^0 \to \tau\tau$, where each τ-lepton is assumed to decay in the 3-prong channel $\tau^- \to h^- h^+ h^- \nu_\tau$. The other decay is the lepton flavor violating decay $B_s^0 \to \mu^\pm \tau^\mp$ combined with the τ-lepton decaying $\tau \to$ 3-prong. This second decay is extremely rare within the SM, but has an enhanced branching fraction in some models beyond the standard model ([6]). It has a somewhat simpler decay topology and its study is straightforward once the reconstruction of the first decay is understood. The methods themselves are presented on a general level and can be applied to other cases with similar decay topologies such as the Higgs boson decay $H \to \tau^+ \tau^-$. Since in the analysis some knowledge about the kinematics of two-body decays will be applied, two-body decays will be discussed on a general level. The insights gained by studying their kinematics will then be applied to show that there exists a possibility to reconstruct the described decays. This will be done on a formal level. The reconstruction as such is more complicated and will only be done numerically. The different versions of the methods will as far as possible be discussed analytically.

In one of the methods first the B_s^0 decay and afterwards the missing particles will be reconstructed. This reconstruction order will be called *bottom up*. In the other two methods this will be the other way around, first the missing particles are computed and then the B_s^0 reconstruction will be done. In this case the reconstruction order is called *top down*. In all reconstruction methods the reconstruction of the B_s^0 vertex will be the crucial task. In principle there are only very rough restrictions on the

possible location of this vertex. The topology of the decay $B_s^0 \to \tau^- \tau^+$ leads to an *area* where the decay could have happened, in the decay topology of $B_s^0 \to \mu^{\pm} \tau^{\mp}$ the vertex must be found on a *line*. This motivates the following names for the reconstruction methods: Bottom Up Areasearch (BUA), Top Down Areasearch (TDL) and Top Down Linesearch (TDL). The names refer to the order of reconstruction and the decay topology required in the corresponding method.

3.1   Two Body Decay Kinematics

The key property of a two-body decay is, that in the restframe of the decaying particle there is only one free parameter (and three masses). Due to energy- and momentum conservation, the momenta of the decay products must be balanced to zero. So obviously stringent constraints for the possible momenta of the particles are obtainable. Furthermore assuming the masses of the involved particles it is possible to compute the energy and the absolute value of the momenta of the decay products. At this point it is important to point out, that what will be referred to as two-body decay must not necessarily be a true two-body decay, but can be a generalized notion of a two-body decay. From a kinematical point of view, the study of a two-body decay can be similar to a decay with more than two decay products. This can be understood when two systems are defined by combining all the decay products into two disjoint sets of particles. Each system can then be regarded as a single particle. The momentum of one system is the sum of the momenta of its constituting particles and the mass of the system is simply the invariant mass of the particles together. For those two systems the same kinematical constraints as for the two daughters in a true two-body decay hold. Thus such a decay can be regarded as a generalized two-body decay. An example for this situation, which will be used later on, is the 3-prong decay of a τ-lepton

$$\tau^- \to h^- h^+ h^- \nu_\tau.$$

By combining the three members constituting the 3-prong into a system and regarding the neutrino as the other system, the 3-prong decay of the τ-lepton can be treated as if it was a two-body decay.

As mentioned above the most obvious properties of a two-body decay reveal themselves in the restframe of the mother particle. From now on this frame will be referred to as the *restframe*. First some variables and the indices of the particles will be defined in the restframe. Only in a second step the decay will be considered in a more general frame by performing a Lorentz transformation. Such a frame will represent the restframe of the detector in an experiment and will be referred to as the *labframe*. The initial particle from now on will be called *mother* and labeled with index 1, whereas the two decay products will be called *daughters* and labeled with indices 2 and 3, respectively. The situation for both frames are schematically illustrated in Figure 3.1.

A two-body decay is bound to a plane, so without loss of generality the coordinate system is chosen such that the decay takes place in the x-y-plane. An arbitrary four

vector a in the decay plane in these coordinates will be denoted as $a = (a_0, a_x, a_y, 0)$. The absolute values of the momenta and energies of the daughters in the restframe are fixed by the masses of the involved particles by the subsequent formulas. Let m_1, m_2 and m_3 be the masses of these particles, then apart from the trivial formula $E_1 = m_1$ the following equations hold[1]:

$$E_2 = \frac{m_1^2 + m_2^2 - m_3^2}{2m_1},$$
$$E_3 = \frac{m_1^2 + m_3^2 - m_2^2}{2m_1}, \tag{3.1}$$

where E_1, E_2 and E_3 are the restframe energies of the corresponding particles. The absolute values of the momenta of the two daughters have both the same value. It is determined by

$$p^2 = E_2^2 - m_2^2 = \left(\frac{m_1^2 + m_2^2 - m_3^2}{2m_1}\right)^2 - m_2^2. \tag{3.2}$$

So in the decay there is only one variable left to define, the orientation of the daughter momenta in the plane. This direction will be referred to as *decay direction*. A direction in two dimensions is given by only one parameter. We define the decay direction by the opening angle between the x-coordinate and the momentum of the particle with index 2. Summing up there are four degrees of freedom, the three masses of the involved particles and the decay direction. In the restframe the whole decay can be described by those four variables.

In a next step a Lorentz transformation to the labframe is performed. The labframe represents an arbitrary inertial frame. Due to momentum conservation also in the labframe the three momenta of the involved particles must be within a plane. The labframe is chosen such that its x-y-plane coincides with the decay plane. So the Lorentz transformation is performed within this plane. This implies that the transformation from the restframe to the labframe introduces only two new variables. The additional variables are the boost direction of the Lorentz transformation and the relativistic factor β. Note that again the direction is fixed by only one variable, since the decay takes place in a plane.

The two additional variables stand in a one-to-one relation to the direction and the absolute value of the momentum carried by the mother particle. This will be shown in section 3.3.2. Of course the direction for the Lorentz boost and the momentum of the mother particle are the same. The absolute value of the momentum of the mother particle p_1 is connected to β via the following formula:

$$\beta = \sqrt{\frac{1}{\left(\frac{E_1}{p_1}\right)^2 - 1}}.$$

---

[1]in all formulas the velocity of light will be set to one, $c = 1$

In order to keep the subsequent equations as simple (and thus as instructive) as possible, in the labframe the mother particle is assumed to fly in the direction of the x-coordinate before it decays. In this case the matrix of the Lorentz transformation from the restframe into the labframe is

$$\Lambda = \begin{pmatrix} \gamma & \gamma\beta & \\ \gamma\beta & \gamma & \\ & & 1 \end{pmatrix}, \tag{3.3}$$

where $\gamma = 1/\sqrt{1 - \beta^2}$ is the usual relativistic boost factor. The explicit form of the Lorentz vectors of the daughter particles in the restframe are defined as

$$\begin{aligned} p_2 &= (p_{20},\ p_{2x},\ p_{2y}) = (E_2,\quad p\cos(\varphi),\quad p\sin(\varphi)), \\ p_3 &= (p_{30},\ p_{3x},\ p_{3y}) = (E_3, -p\cos(\varphi), -p\sin(\varphi)), \end{aligned} \tag{3.4}$$

where the unused third spacial dimension is left away. With this definitions it is easy to compute the Lorentz vectors of the particles in the labframe. Using equations (3.3) and (3.4) it follows that

$$\begin{aligned} p_2' &= \Lambda\,p_2 = (\gamma\,(E_2 + \beta p\cos(\varphi)),\ \gamma\,(\beta E_2 + p\cos(\varphi)),\quad p\sin(\varphi)), \\ p_3' &= \Lambda\,p_3 = (\gamma\,(E_3 - \beta p\cos(\varphi)),\ \gamma\,(\beta E_3 - p\cos(\varphi)), -p\sin(\varphi)). \end{aligned} \tag{3.5}$$

In these equations it can be read off directly that the momenta of the daughter particles in the labframe are mainly determined by their restframe decay properties, namely the variables φ, p, E_2 and E_3. The change of coordinates to the labframe introduces only two new parameters: the beta factor β and the direction of the Lorentz transformation. For simplicity in the equations above this direction has been fixed to be the x-coordinate, but it is important to remember that in the general case a rotation into an arbitrary direction introduces one additional variable. The special structure of the momenta of particles originating from a two-body decay, or equivalently combined systems originating from a generalized two-body decay, is what is going to be used in order to make reconstructions of such decays. It is clear that the boost of the mother particle "bends" the momenta of the daughters into the mother's flight direction. The forward bending of the flight direction of the daughters depends on the component of their restframe momentum into the flight direction of the mother, as can be seen in equation (3.5). The situation in the restframe and in the labframe is sketched in Figure (3.1), also schematically illustrating the forward bending of the τ-lepton flight directions by the Lorentz transformation.

3.2   Event Topologies

The following methods all use topological information to reconstruct decays. Therefore the requirements on the topology on a decay, needed such that it is reconstructible by one of the three methods, will be discussed before presenting the actual
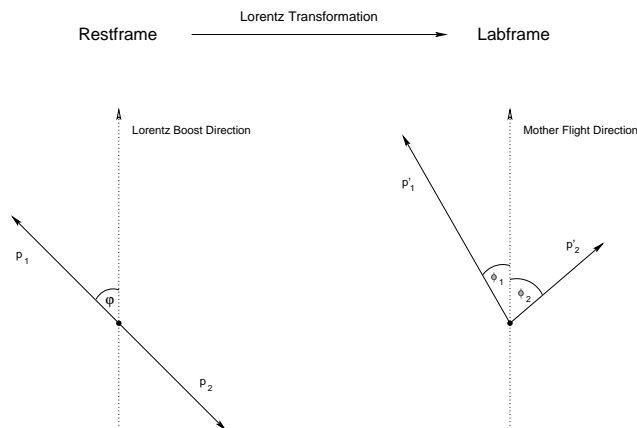
Figure 3.1: Schematic illustration of the situation in the two relevant frames of reference.

methods. There are two possible sets of requirements on the decays such that one of the reconstruction methods becomes applicable. For both sets the basic requirement is, that there must be an initial particle (mother) decaying in a true[2] two-body decay. The difference of the two sets lies in the requirements on the decay products. In one case both daughters are unstable and are assumed to decay into 3-prongs with at least one missing particle in each secondary decay. In the other case only one of the daughters decays in that channel and the other is stable and detectable. The 3-prong decay is interesting because it provides information about the daughter decay vertices and therefore also some information about its flight direction. Since a 3-prong has three tracks originating from the same point in space, in experiments it is possible to reconstruct the intersection-point of the three prong-member tracks. The decay vertices of the daughters can then be identified with this measured point in space. In one decay topology the measurement of the decay vertices will provide the necessary topological information needed to successfully reconstruct decays with the subsequent methods. In the other decay topology the information that can be exploited for the reconstruction is the flight direction of the stable particle involved and the single vertex from the 3-prong. Despite the loss of information about energy and momentum due to the missing particles, the reconstruction of the decays is possible.

In the following sections equation (3.5) will play an important role, and so it is important to point out that in this equation the flight direction of the mother particle was fixed to be in the x-coordinate. In the discussed decay topology the mother decay vertex is unknown. But in order to apply equation (3.5) the decay vertex of the mother particle, which also includes the information about its flight direction, must be known. The determination of this vertex will be the crucial task in the

---

[2]and *not* in a generalized two-body decay as it is defined in Section 3.1

presented reconstruction methods.

3.2.1   Topology with two 3-prongs

In this case the two daughter particles both decay in a 3-prong and one missing particle. Each 3-prong will indicate a decay vertex. These two measured vertices are denoted as $\vec{v}_2$ and $\vec{v}_3$ (the labeling of the particles is the same as in Section 3.1). That means that there exists another vertex $\vec{v}_1$ from which both particles decaying at the vertices $\vec{v}_2$ and $\vec{v}_3$ originated. Of course this vertex is then the mother decay vertex. The decay topology is sketched in Figure 3.2. In the figure the 3-prong systems are summarized into large arrows in order to illustrate the generalized two-body decays, where the visible 3-prong part and the missing particle are regarded to form a quasi two-body decay. There is only one very simple and rough restriction on the location of the mother decay vertex: considering momentum conservation, it is easy to understand that it must lie within the triangle that has its corners at the mother production vertex and the two daughter decay vertices. This has been illustrated in Figure 3.2. Most often both labframe decay angles ϕ_1 and ϕ_2 will be smaller than $\pi/2$. This is because in a realistic experimental set-up the mother particles will almost always have high momenta and thus the daughters are strongly boosted. So in the labframe they tend to fly into the same direction as the mother particle. This can be understood by looking at the component of the daughter momenta into the mother flight direction. The formula for this value in the labframe can be extracted from equation (3.5) and is given by

$$p'_{2,3} = \gamma\left(\beta E_{2,3} \pm p\cos(\varphi)\right),$$

which can only be negative for small β and will increase substantially for β close to one. Since $E_{2,3} \geqslant p$ always holds, for β close to one the momentum component $p'_{2,3}$ is positive for all decay angles φ and thus $\phi_{1,2} < \pi/2$.

3.2.2   Topology with one 3-prong and one stable particle

In the case with only one 3-prong and one stable particle, the situation is much simpler. An illustration for the simpler decay topology is given in Figure 3.3. In collider experiments stable particles such as muons provide a clear track. This track can be extrapolated through the production vertex of the stable particle. In the present case this vertex will coincide with the unknown mother decay vertex. This implies that the allowed space where the mother decay vertex could possibly be located is a line instead of an area as before. Apart from that difference the two decay topologies can be treated quite similarly. So the reconstruction of decays with one stable particle can be derived almost as a special case of the more complex case with two unstable daughters. Instead of the area within the triangle as possible positions for the mother decay vertex, there is now a line on which the vertex must be found.
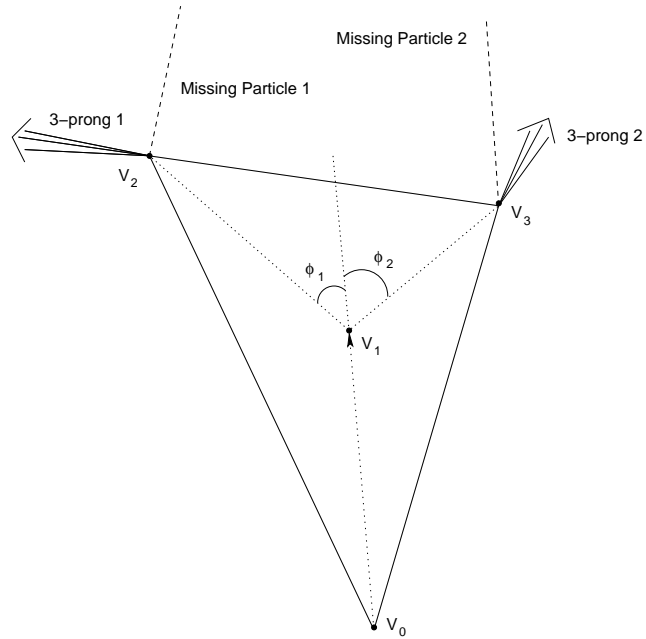
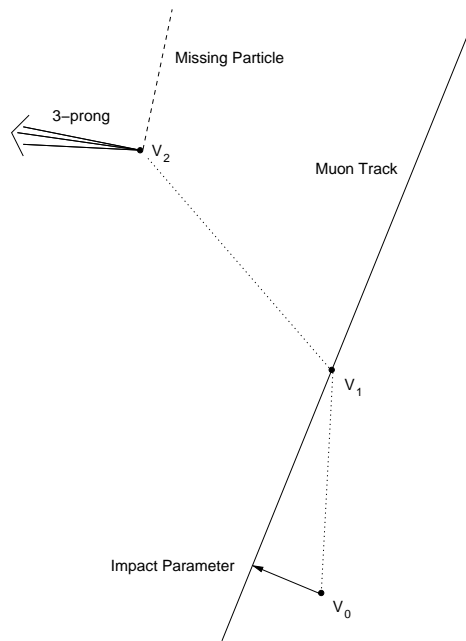Figure 3.2: Decay topology with a triangle of possible hadron decay vertices.

Figure 3.3: Decay topology where the solution is bound to a Line.

3.3   Reconstruction Methods

When trying to develop a reconstruction method applying the properties of two-body decays, there are several possible approaches which in their own sense are instructive and have specific advantages. In this section the basic ideas of three different approaches will be discussed. The discussion of these different approaches will be kept as general as possible. Applications of the methods to the corresponding specific cases are postponed to Chapter 4. The three presented methods are labeled Bottom Up Areasearch (BUA), Top Down Areasearch (TDA) and Top Down Linesearch (TDL). Note that the basic idea behind all three methods is the same, namely to make use of the special properties of two-body decays and their decay topology. All the methods are inspired by the Neutrino Reconstruction Method (NR) which was first presented in [7]. The NR is a crucial ingredient for the methods TDA and TDL.

In the BUA method first the momenta of the daughters of the mother particle are reconstructed and then the missing parts in the 3-prongs are computed. Compared to the BUA, in the TDA and the TDL the order of reconstruction is going to be reversed. There the first step is to reconstruct the missing part in the 3-prong decays and only then the momenta of the daughter particles are reconstructed. This direct reconstruction of the missing 3-prong part is done using the NR. Before applying it to the present decay topologies, the NR will be discussed shortly in the next section. A detailed discussion of the NR method and a different application than the application in this work is given in [7].

3.3.1   Neutrino Reconstruction

The reconstruction of a missing particle in a decay according to the NR is based on the knowledge of topological information. For simplicity within this section the reconstructed decay is a 3-prong decay and the missing part is assumed to be a neutrino. The topological information needed to reconstruct a neutrino is the flight direction of the mother particle. Once this direction is given, the momentum of the visible part of the decay is divided into a perpendicular- and a parallel component with respect to the flight direction. These components are denoted as $p'_\perp$ and $p'_\parallel$. The separation into perpendicular- and parallel components of the visible decay part is illustrated in Figure 3.4. Note that these two components are precisely the two components of one of the vectors in Equation (3.5). So these components are already known and given by

$$
\begin{aligned}
p'_\parallel &= \gamma \left(\beta E + p \cos(\varphi) \right), \\
p'_\perp &= p \sin(\varphi),
\end{aligned}
\tag{3.6}
$$

where p and E are the energy and the momentum of the visible 3-prong part in the restframe, γ and β are the usual relativistic boost factors, and φ is the decay angle of the visible 3-prong system in the restframe with respect to the mother flight

direction. As discussed in Section 3.1, the energy and the momentum depend only on the masses of the involved particles. This means that if these masses are known, Equations (3.6) provide two conditions for the two unknown variables φ and β. The determining equations for those two values are

$$
\begin{aligned}
\frac{p'_\perp}{p} &= |\sin(\varphi)|, \\
0 &= (E^2 + p^2 \cos(\varphi)^2) \cdot \beta^2 + 2\,E\,p\cos(\varphi)\cdot\beta + (E^2 - E'^2),
\end{aligned}
\tag{3.7}
$$

where E' is the energy of the visible 3-prong part in the labframe and the other variables are defined above. Note that the equation determining β is a quadratic equation which will provide two different solutions, and also for φ there are two solutions whenever $p \neq p_\perp$. Mostly one of the two solutions for β arising due to the quadratic equations will not satisfy the physical condition $0 < \beta < 1$ and can be discarded. The two solutions for φ arise because the first equation in (3.7) only provides an absolute value for $\sin(\varphi)$. This is because in the labframe it is almost never possible to know whether the visible part decayed in the mother flight direction (forward) or against the flight direction (backward). The only case where the two solutions can be distinguished is when $p'_\parallel < 0$. In this case the visible part was backward scattered. But whenever the mother particle is strongly boosted, $p'_\parallel$ will be positive. This is due to the fact that $E > p$ and thus for β close to one, the parallel component in Equation (3.6) will be positive. In experiments this is almost always the case.

The two possible solutions from the NR give rise to combinatorial background. One of the solutions is always the true solution, but it is not possible to know which one it is and thus both solutions have to be considered. This fact will broaden the distributions of all the reconstructed variables. So the difference between the two solutions is discussed shortly below, although for the present work this will not be used. The difference of the two solutions is given by

$$
|\Delta p'_{reco}| := \left|\vec{p}\,'_1 - \vec{p}\,'_2\right| = 2\,\gamma\,p\,|\cos(\varphi)|\,.
$$

So the absolute value of the difference of the two solutions goes to zero for $\varphi \to \pi/2$. Note that the difference of the two solutions lies only in the parallel component $p_\parallel$, the perpendicular component is the same for both solutions. Moreover since both the absolute value of the true solution p' and the difference of the two solutions are proportional to γ, even in the limit $\gamma \to \infty$ the relative error due to the two solutions is finite:

$$
\begin{aligned}
\frac{|\vec{p}\,'_1 - \vec{p}\,'_2|}{|\vec{p}\,'_{1,2}|} \leqslant \lim_{\beta \to 1} \frac{|\vec{p}\,'_1 - \vec{p}\,'_2|}{|\vec{p}\,'_{1,2}|} &= \lim_{\beta \to 1} \frac{2\gamma p\,|\cos(\varphi)|}{\sqrt{\gamma^2(\beta E \pm p\cos\varphi)^2 + p^2\sin\varphi^2}} \\
&= \lim_{\beta \to 1} \frac{2 p\,|\cos(\varphi)|}{\sqrt{(\beta E \pm p\,|\cos\varphi|)^2 + (p^2\sin\varphi^2)/\gamma^2}} \\
&= \frac{2 p\,|\cos(\varphi)|}{E \pm p\,|\cos\varphi|} \leqslant \frac{2}{(E/p) - 1} < \infty,
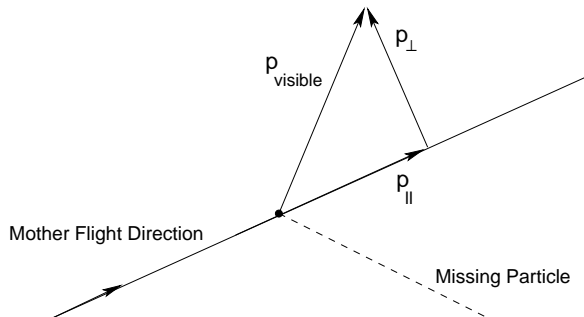\end{aligned}
$$

Figure 3.4: Topological Neutrino Reconstruction.

where $\vec{p}\,'_{1,2}$ denote the two different solutions for the momentum in the NR. The deviation of the wrong solution from the true one becomes small for large restframe decay angles $\varphi \sim \pi/2$. Moreover the relative error is bounded from above. A total upper bound and an upper bound that depends only on the decay angle have been given.

3.3.2   Bottom Up Areasearch

This variant of the reconstruction method is used to reconstruct decays containing two 3-prongs. The topology of these decays is described in Section 3.2.1 and illustrated in Figure 3.2. The reconstruction of such decays will be done by directly computing the Lorenz vectors of the two daughters for each possible decay vertex of the mother. Due to momentum conservation, the decay vertex is bound to the triangle spanned by the primary vertex and the daughter decay vertices. Without loss of generality, the primary vertex $\vec{v}_0$ is assumed to be at $\vec{v}_0 = 0$ and the vectors pointing to the decay vertex of the two daughters are denoted as $\vec{v}_2$ and $\vec{v}_3$. In a case where $\vec{v}_0$ is not equal to zero, one can simply shift the coordinate system by $\vec{v}\,'_{2,3} = \vec{v}_{2,3} - \vec{v}_0$ and then $\vec{v}\,'_0 = 0$. The two daughter decay vertices and the primary vertex will be measured in experiment for each decay and as such they are input parameters for the reconstruction algorithm. So for the present calculation they are assumed to be known parameters. Furthermore the mother decay vertex candidate will be denoted as $\vec{v}_1$.

For each fixed mother decay vertex candidate $\vec{v}_1$, the flight directions of the decay products are $\vec{v}_2 - \vec{v}_1$ and $\vec{v}_3 - \vec{v}_1$, respectively. The parametrisations of the labframe decay angles ϕ_1 and ϕ_2 in terms of $\vec{v}_1$ are defined through the following expressions:

$$
\begin{aligned}
\phi_1(\vec{v}_1) &= \arccos\left(\frac{(\vec{v}_2 - \vec{v}_1) \cdot \vec{v}_1}{|\vec{v}_2 - \vec{v}_1|} \right) \\
\phi_2(\vec{v}_1) &= \arccos\left(\frac{(\vec{v}_3 - \vec{v}_1) \cdot \vec{v}_1}{|\vec{v}_3 - \vec{v}_1|} \right).
\end{aligned}
$$

In order to reconstruct the decay it is necessary to connect the labframe decay angles to the variables determining the Lorentz vectors of the daughters. So the two labframe decay angles will also be expressed in terms of the kinematical variables β and φ using Equation (3.5). In these equations the flight direction of the mother particle is fixed to be the x-coordinate and so by simply dividing the x- and y-components the angles can be expressed as

$$\cotan\big(\phi_{1,2}(\beta,\varphi)\big) = \frac{p'_x}{p'_y} = \frac{\gamma(\beta E_2 \pm p\cos(\varphi))}{p\sin(\varphi)}. \tag{3.8}$$

As a next step Equation (3.8) must be solved for β and φ in order to obtain expressions for those values in dependence of the two labframe decay angles $\phi_{1,2}$. This will be done using the simple form of the equations. In equation (3.8) ϕ_1 and ϕ_2 only differ by the sign of a term within the equation, motivating the following definitions

$$
\begin{aligned}
R_1 &:= \cotan(\phi_1), \\
R_2 &:= \cotan(\phi_2), \\
R_+ &:= R_1 + R_2, \\
R_- &:= R_1 - R_2
\end{aligned}
\tag{3.9}
$$

If we express β and φ in terms of these variables the resulting equations take a surprisingly simple form. The variable β is then determined by a polynomial equation of fourth degree. This polynomial equation is equivalent to a quadratic equation because it does not contain odd terms. For a given β obtained by the quartic equation, also the formula for the restframe decay angle takes a simple form. Both expressions are shown in the subsequent equation.

$$
\begin{aligned}
&R_-^2\, m_1^2\, \beta^4 - \left[m_1^2(4+R_-^2) + 4R_+^2\, p^2\right]\beta^2 + 4R_+^2 p^2 = 0, \\
&\sin(\varphi) = \frac{\gamma\beta m_B}{R_+ p},
\end{aligned}
\tag{3.10}
$$

where m_1, p, γ and β are defined in Section 3.1 and $R_\pm$ in Equation (3.9). For a given $\vec{v}_1$ it is now possible to compute the necessary kinematical variables β and φ needed to reconstruct the decay analytically. This can be done by substituting $R_\pm$ in Equation (3.10) by the variables in Equations (3.8) and (3.9). Once these variables are known, they can be used to evaluate Equation (3.5) and thus compute the reconstructed Lorentz vectors of the daughter particles.

Note that Equation (3.10) provides at most four formal solutions for β. Two of these solutions will always be negative and can be discarded immediately. A comparison to the simulated data shows that in most practical cases, in Equation (3.10) there is only one physical solution where $0 < \beta < 1$.

For each fixed mother decay vertex candidate $\vec{v}_1$ the values of β and φ can now be computed using the two previous equations. Therefore the two daughter particles can be reconstructed for each mother decay vertex candidate $\vec{v}_1$. Since $\vec{v}_1$ is a vector in a plane, there are two remaining degrees of freedom in the equations

that formally determine the decay. It is then clear that in order to reconstruct the whole decay without knowing the true $\vec{v}_1$, two restrictions are needed. Two restrictions will allow to find isolated solutions for $\vec{v}_1$. These restrictions can be gained by combining the reconstructed daughters and the measured 3-prong momenta. Recall that the daughters of the initial particle are assumed to decay into a 3-prong. But if the decay channel of the daughter particles is assumed fixed, also the mass of the invisible part in the prong is fixed. In the main example $B_s^0 \to \tau\tau$ this invisible part will be the neutrino produced in the decay of each daughter particle. Since the 3-prong momenta can be measured, two restrictions are obtained by simply subtracting the Lorentz vectors of the 3-prong system from those of the corresponding reconstructed daughters. Due to four-momentum conservation, this difference must be the Lorentz vector of the missing part of the decay. Hence the invariant mass of this reconstructed four vector must be equal to the invariant mass of the missing 3-prong part. This mass is known by assuming certain decay channels of the daughters. Putting all this together a system of equations is obtained that can formally be written as

$$
\begin{aligned}
(p_2'(\vec{v}_1) - p_{3prong,1})^2 &= m_{miss,1} \\
(p_3'(\vec{v}_1) - p_{3prong,2})^2 &= m_{miss,2},
\end{aligned}
$$

where p_2', p_3' and $\vec{v}_1$ are defined above, $p_{3prong,1}$ and $p_{3prong,2}$ are the measured Lorentz vectors of the two 3-prongs and finally $m_{miss,1}$ and $m_{miss,2}$ are the invariant masses of the invisible parts of the decay. Assuming the masses of the involved particles, the above expressions are two equations for two unknown variables. So in principle the system of equations remains to have zero degrees of freedom and should provide isolated solutions for the possible mother decay vertex $\vec{v}_1$. Although these formal restrictions have a very simple form, the expressions are not yet solved for the unknown vector components of $\vec{v}_1$. Their dependence on the measured quantities $p_{3prong1,2}$ is not simple and can not be computed analytically. The solutions for $\vec{v}_1$ will only be obtained numerically.

The chosen algorithmic implementation of the BUA method is a simple gridsearch within the triangle of possible decay vertices $\vec{v}_1$. After defining a grid in the area of the triangle, for each point on the grid the mass of the reconstructed neutrinos is computed by the formulae above. The gridpoint with the smallest neutrino masses is kept as solution.

The name of the Bottom Up Areasearch method can now be motivated: in this method the initial particles are reconstructed first using the geometrical properties of two-body decays, and only then the final states are computed. In the Top Down Areasearch presented in the next section the order of reconstruction will be reverted and it will be possible to make the reconstruction with less input parameters. The BUA method has only been applied in order to illustrate the possibilities one has with this approach and make a proof of concept (see Section 4.1). A more detailed analysis of the decay $B_s^0 \to \tau\tau$ will be made in Section 4.3 applying the Top Down Areasearch. In order to offer an alternative explanation of the BUA, the reconstruc-

tion algorithm is written in pseudo-code:

1. define a grid in the triangle

2. at each gridpoint do

   (a) compute labframe decay angles

   (b) reconstruct the daughter momenta using the decay angles

   (c) P = subtract the daughter momenta from the 3-prong momenta

   (d) ThisMass = compute mass of P

   (e) if ThisMass < MinimalMass

       i. MinimalMass = ThisMass
      ii. BestPoint = This Gridpoint

3. reconstruct decay at BestPoint

4. store reconstructed variables

3.3.3 Top Down Areasearch

So far the BUA reconstruction method and a possibility to reconstruct decays with missing particles was presented. It will be shown in Section 4.1, that the BUA most often reconstructs the decay vertex of the mother particle to a high precision, as long as the mass of all the involved particles are assumed to be known and can be used as input parameters. The problem with the BUA method is, that for background events with similar decay topologies, this algorithm will often reconstruct a hypothetical decay vertex. Since the mass of the initial particle is an input parameter, the mass can not be used in the analysis as a variable to distinguish reconstructed background events from reconstructed signal events. But for many practical cases the other kinematical variables of background events are quite similar to those of signal decays. This means that the BUA method will have very small signal over background ratio in these situations because the efficiency on background will be comparable to the efficiency on signal. This problem can be overcome with the Top Down Areasearch (TDA) reconstruction method discussed in the present section. It does not take the mass of the initial particle as an input parameter, but the mass is rather going to be reconstructed by the algorithm. This is a great advantage the TDA has over the BUA method and it is the reason why a more detailed analysis of an example is only performed using the TDA method. The discussed example will be the decay $B_s^0 \rightarrow \tau\tau$.

The decay topology of the decays that can be reconstructed with the TDA method is the same as in the BUA method where both daughters decay in the 3-prong channel. This topology has been presented in Section 3.2.1 and is displayed in Figure 3.2. To get isolated solutions for the mother decay vertex in a decay with this topology,

the masses of all involved particles had to be assumed, as shown with the BUA method in Section 3.3.2. The relinquishment of using the information about the mass of the mother particle will introduce one degree of freedom into the equations that determine the decay. So instead of isolated solutions, for each event there is a one-dimensional set of possible mother decay vertices. Because of that, the reconstruction of the events becomes more complicated and the reconstruction of the mother decay vertex will not be unambiguous.

Recall that even using the mass of the initial particle the reconstruction of the correct decay vertex could only be done numerically. Thus it is clear that the reconstruction without fixing the mass of the mother particle can even more so only be made numerically. Therefore it is necessary to explain how to compute a variable which then can be optimized numerically. The way to achieve such a variable is physically motivated, the optimization itself is a purely numerical problem. So the description of the reconstruction algorithm will be divided into two parts. In a first step the way to compute an optimization variable will be presented. In a second step the numerical handling of the problem will be discussed.

Physical Reconstruction

The goal of the physical reconstruction is to provide a variable which can be optimized numerically. Recall that in the BUA method such a variable was also proposed. There the procedure was to compute the masses of the missing particles in the decay for a given mother decay vertex candidate. These masses were then approximated to the assumed masses of the missing particles. The procedure was to minimize the difference between the reconstructed and the assumed mass over many different mother decay vertex candidates.

Also in the TDA method a variable will be proposed which has to be minimized numerically. For a fixed mother decay vertex $\vec{v}_1$, the flight direction of the daughter particles are also fixed and given by $(\vec{v}_2 - \vec{v}_1)$ and $(\vec{v}_3 - \vec{v}_1)$ as can be seen in Figure 3.2. Once the flight direction of the daughters is fixed, the NR can be applied and the Lorentz vectors of the two daughters can be computed. Moreover since the mother particle is assumed to be produced at the primary vertex, the mother vertex vector also indicates the mother flight direction. This immediately leads to a very simple and intuitive restriction for the reconstructed variables: since it is assumed that the two daughter particles originate from a two body decay, their momenta must be balanced with respect to the mother flight direction. So for each mother decay vertex the momenta of the daughter particles can be computed and their component perpendicular to the mother flight direction can be compared. In a formula this restriction can be written as follows

$$\Delta p_\perp(\vec{v}_1) := \left| p'_{\perp,2}(\vec{v}_1) - p'_{\perp,3}(\vec{v}_1) \right| \overset{!}{=} 0,$$

where $p_{\perp,2}$ and $p_{\perp,3}$ denote the perpendicular components of the reconstructed daughter momenta with respect to the associated mother flight direction. This

restriction is the only requirement that can be put on the reconstructed daughter momenta. Whenever the above condition is satisfied, the corresponding momenta could be a product of a two body decay. All the properties of two body decays discussed in Section 3.1 are satisfied. The invariant mass of the hypothetical mother particle is then the invariant mass of the sum of the two daughter Lorentz vectors. Now it becomes clear why the degree of freedom in the system without assumptions about the mother mass is equal to one. The mother decay vertex candidate has two variables, since it is a vector in a plane. But there is only one possible restriction on the two variables, namely the balance $\Delta p_\perp(\vec{v}_1) \overset{!}{=}$ of the corresponding reconstructed daughter momenta. So for each decay that has to be reconstructed, a one-dimensional set of mother decay vertices is obtained. For each vertex from this set the invariant mass of the mother candidate can be computed. This implies that for each event there is a spectrum of possible masses for the mother particle. This leads to a special kind of error on the reconstruction. However this mass spectrum must contain the true mass, since the true decay vertex also satisfies the balancing condition. In the discussion of the example decay $B_s^0 \to \tau\tau$ it will be shown that unbiased estimators can be achieved despite the uncertainty due to the set of solutions.

Some other combinatorial problems appear because the NR is applied twice in the reconstruction. As it is explained in section 3.3.1, there is already a two fold ambiguity in the reconstruction of the daughter momenta. But since in each decay the NR is applied twice, for each mother decay vertex candidate there are four momenta of the daughters, two for each single daughter. These four reconstructed momenta can be combined in four different ways. For all four combinations of the daughter momenta the above discussion applies. The different solutions of the NR can be understood physically as forward- and backward decays of the 3-prong in the decay of the daughters. So the four combinations of the reconstructed momenta can be ordered according to this interpretation and thus for each combination $\Delta p_\perp(\vec{v}_1)$ can be optimized separately.

Numerical Approximation

The physical reconstruction has lead to a discriminating variable $\Delta p_\perp(\vec{v}_1)$ which can be computed for each mother decay vertex $\vec{v}_1$. For a fixed $\vec{v}_1$ this variable can be computed separately for the four different combinations of the four reconstructed daughter momenta. All four combinations can be treated as completely independent. The subsequent numerical approach to the problem will be applied in the same way to each combination. So in the following discussion of the numerical handling of each event, this ambiguity will be left aside.

It was argued that the condition that the momentum balance $\Delta p_\perp(\vec{v}_1) \overset{!}{=} 0$ is the only available constraint on the mother decay vertex candidates. But since $\vec{v}_1$ is a vector in a plane, there remains one additional degree of freedom in the system of equations determining the mother decay vertex. In principle each event contains an infinite set of candidates which all satisfy the only given condition. This leads

to the conclusion that a simple minimization of $\Delta p_\perp(\vec{v}_1)$ does not necessarily produce the true decay vertex, but rather an arbitrary point out of the set of possible solutions. In principle all the points within this set of candidates have perfectly balanced momenta but varying candidate mother masses. So if vertices out of this set are approximated, any deviation of $\Delta p_\perp$ from 0 must have a numerical nature. Such a difference occurs only due to the fact that these points are numerically approximated.

But then a very practical problem arises: it is impossible to store a continuous set of decay vertex candidates. If there is any hope to achieve a reasonable reconstruction algorithm, within each event a choice has to be made on which vertex candidates are going to be stored. Since there is no physical discriminant to make such a choice, the goal must be to choose a mother decay vertex candidate which is stable against different numerical proceedings. This will be done by taking an average over the set of solutions. Recall that for each mother decay vertex candidate there is an associated mass of the reconstructed mother particle. So in principle an average mass over the set of possible vertex candidates can be computed for each decay. The candidate that is stored is the candidate whose associated mass is equal to the average mass. Two reasons can be given why this is a good choice for the mother decay vertex candidate:

- The first reason is that formally the point with the average invariant mass is a definite property of each specific decay. It is a fixed point and should not depend on the numerical approach.

- The second reason is simply its existence. Without knowing the mass of the mother particle, it is impossible to guess a specific mass value which is contained within the mass spectrum along the line of solutions. It is old and solid mathematical knowledge that the mean value of a continuous set is also contained in the set itself. So in order to work independently from the mass of the initial particle, the mean value of all the reconstructed masses is a good quantity to work with.

In order to compute the average mass of the set of vertex candidates a numerical approximation to this set has to be proposed. The rest of this section will be dedicated to the technical details of the numerical approximation. The candidates constituting the set of mother decay vertices all satisfy the condition $\Delta p_\perp(\vec{v}_1) = 0$ and thus it is obvious that this condition has to be fulfilled by each interesting vertex candidate. In order to find vertex candidates satisfying that condition the Minuit minimization package will be used. The simple grid minimization procedure from the BUA is replaced by the well known and numerically more powerful Migrad algorithm from the Minuit package. This package is implemented in the ROOT environment and can be used straightforwardly as soon as a minimization function has been defined. As an input parameter Migrad needs a starting point. From a given starting point Migrad tries to find a local minimum of the given function which has to be minimized. For the present case this means that Migrad will converge to

a mother decay vertex candidate which satisfies $\Delta p_\perp(\vec{v}_1) \sim 0$ and is located near the given starting point. The convergence point is an approximation to an arbitrary point from the set of mother decay vertex candidates. In order to find as many such approximate vertex candidates as possible, a set of starting points has to be defined. This will be done by defining a grid of starting points which are all placed within the triangle limited by $\vec{0}$, $\vec{v}_2$ and $\vec{v}_3$ (see Figure 3.2). Note that the NR does not necessarily provide solutions for each point within that triangle. So before using a gridpoint as starting point for Migrad, first the NR is applied at that starting point. If a solution exists, the starting point is defined as *good starting point*. Only from the good starting points Migrad is run. Whenever Migrad converges, the convergence point is stored temporarily. This provides a set of convergence points which all approximately satisfy the condition $\Delta p_\perp(\vec{v}_1) \sim 0$. But this is not yet a good approximation to the desired set of mother decay vertex candidates. The problem is that these convergence points are not regularly distributed along the true set of vertex candidates. To avoid a biased numerical weighting of the set of vertex candidates, the given triangle is divided into segments. Each segment is then either marked when it contains at least one convergence point, or remains unmarked when it contains no convergence point. In that way a segment containing many convergence points is not overweighed compared to other segments containing less starting points. Finally all marked segments together can be regarded as a good approximation to the one-dimensional set of mother decay vertex candidates.

The average mass m_{mean} of the decay needed to choose a single vertex candidate is computed as follows. For one vertex candidate in each marked segment (i) the mass of the corresponding mother particle m_i is reconstructed. Then all the masses of the marked segments are summed up and this sum is then divided by the total number of marked segments N:

$$m_{mean} = \frac{1}{N} \cdot \sum_{i=0}^{N} m_i.$$

The coordinates of the segment with the corresponding invariant mass which is closest to the mean value m_{mean} determine the mother decay vertex candidate which is finally stored. Recall that this procedure is applied to the four combinations from the NR. There are events where some combinations do not provide any convergence points at all and do not provide a vertex candidate to store. However for most events all four combinations contribute one mother decay vertex candidates to be stored.

The procedure described above contains the core of the reconstruction algorithm since it describes how each single event is reconstructed. In order to make the procedure clearer and also to offer an alternative to the text above, the whole procedure has also been written in pseudo-code:

```
for each combination do

  1. determine starting points
```

2. segmentate area

3. for each starting point do

    (a) run minuit from starting point

    (b) if convergence, mark segment at the convergence point

4. for all segments do

    (a) if segment is marked

        i. newmass = reconstructed mass at this segment

       ii. summass = summass + newmass

      iii. counter++

5. meanmass = summass/counter

6. meansegment = find segment with mass closest to meanmass

7. reconstruct at meansegment

8. store reconstructed variables

3.3.4 Top Down Linesearch

In some aspects of the methods, the Top Down Linesearch (TDL) can be regarded as a special case of the TDA. The physical approaches used to reconstruct events are very similar in both cases. Their main difference lies in the decay topologies that can be reconstructed by the two approaches. While the TDA reconstructs events with a two-body decay which is followed by two 3-prong decays of the daughter particles, the TDL provides a possibility to reconstruct decays where one of the daughter particles is stable and detectable. The decay topologies are discussed in Section 3.2.2 and sketched in Figure 3.2.

When one daughter is stable, it is possible to measure its three-dimensional momentum and its track. Since the daughter is a direct decay product of the mother particle, this track will point to the decay vertex of the mother. The track is determined by its impact point and the momentum direction of the muon. So a line is obtained on which the mother decay vertex must be found. For each mother decay vertex candidate on the line, the flight direction of the unstable daughter is fixed. So the NR can be applied. This is similar to the TDA, but now only one of the daughter momenta is reconstructed with the NR, the other can be measured directly. Again the reconstructed momentum components from the NR and the muon momentum with respect to the associated mother flight direction must be balanced:

$$\Delta p_\perp(\vec{v}_1) := \left| p'_{\perp,2}(\vec{v}_1) - p'_{\perp,\mu}(\vec{v}_1) \right| \overset{!}{=} 0,$$

But since the different decay topology only allows possible mother decay vertices on a line, the total degrees of freedom decrease by one compared to the TDA. The

single constraint of balancing the two daughter momenta is sufficient to get two isolated solutions instead of the one dimensional set of solutions from before. There is still a two fold ambiguity due to the two different solutions in the NR, leading to two solutions for the mother decay vertex in each event. However one of these two solutions will always be the true solution. This means that there will still be combinatorial background, but the true value should always be found and the combinatorial background is much smaller than in the TDA.

The optimization of the momentum balance is done using Migrad from the Minuit package. Since also here the NR will not necessarily provide solutions for all possible flight directions, good starting points for the minimization have to be found. A good starting point is determined by the existence of a solution for the NR when the NR is applied to the corresponding daughter flight direction. Note that instead of looking for good starting points in an area, the good starting points have only to be found along the given line. A difference to the TDA is also that now it makes sense to store the mother decay vertex candidate with the best balanced momenta. The true decay vertex will be an isolated solution for the minimization and there is no other point where the balancing can be equally good. So in contrast to the situation in the TDA, the quality of the minimization has also a physical interpretation and is not only a numerical property of the convergence point. So for each combination simply the vertex candidate with the best momentum balance can be stored and one of the two solutions obtained will be the true mother decay vertex. The crucial part of the reconstruction algorithm is again written in a simplified pseudo-code in order to provide an alternative description of the algorithm:

```
for each combination do

  1. segmentate line

  2. determine good starting points

  3. for each good starting point do

     (a) run minuit from starting point

     (b) ΔP = momentum balance at the convergence point

     (c) if ΔP < ΔP_min

         i.  ΔP_min = ΔP

         ii. bestpoint = this convergence point

  4. reconstruct the event at bestpoint

  5. store reconstructed variables
```

Chapter 4

Application of the Reconstruction Methods

In this chapter the presented methods are applied to specific decays in order to illustrate the reconstruction possibilities they provide. Also the concrete realizations of the reconstruction algorithms are discussed. The BUA and the TDA have been applied to the decay $B_s^0 \to \tau\tau$. The TDL has been applied to the lepton flavor violating process $B_s^0 \to \tau\mu$ which is only allowed in some models that go beyond the standard model. The two selected decays are chosen as examples because they have the topologies needed such that the methods are applicable. As discussed in previous sections, the TDA has some important advantages compared to the BUA. Because of that the BUA is only applied to reconstruct events so far that a proof of concept is given, but no analysis is done with this method.

All the used data sets are simulated event samples generated by the Pythia Monte Carlo[1] event generator. The events where generated with a center of mass energy of $E_{CM} = 14$ TeV.

4.1 Proof of Concept for the BUA method

The BUA method has been applied to the decay $B_s^0 \to \tau\tau$. So the involved particles are the B_s^0 as the mother particle, two τ leptons as daughters and ν_τ neutrinos are the missing particles in each tau 3-prong decay. The applied numerical approach to reconstruct the mother decay vertex is a simple grid-search in order to minimize the masses of the reconstructed neutrinos. In the reconstruction algorithm for each point in a grid lying within the limiting triangle of each event, the neutrino Lorentz vectors are computed as explained in detail in Section 3.3.2. The resulting neutrino masses have been chosen to be the reconstructed variable which are minimized for each event. The grid-point where the sum of both reconstructed neutrino masses is minimal is kept as the reconstructed vertex. Note that if the true decay vertex is

---

[1]the applied version is V6.227

Entries	9958
Mean	1.28313
RMS	2.13171
Underflow	0
Overflow	1321

Entries	19916
Mean	0.476605
RMS	0.7906
Underflow	0
Overflow	276
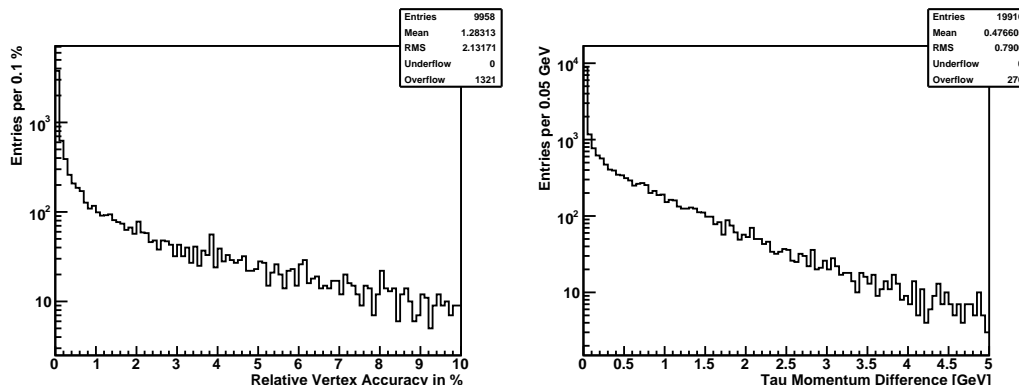
Figure 4.1: Relative accuracy of the reconstructed mother decay vertex v_1 (left), and the resolution of the reconstructed τ-momenta in GeV (right).

given, this reconstruction is analytical. However the decay vertex is not known and so its reconstruction is the crucial task of the reconstruction algorithm. Since in the BUA the mass of the mother particle is assumed fixed (in this case the mass of the B_s^0) the reconstruction should provide isolated solutions. But there is not always a unique solution for the mother decay vertex. Some ambiguity is left and by minimizing the neutrino masses only one of the possible solutions is kept. Therefore the true vertex is not always reconstructed successfully. The reconstruction algorithm has been applied to 10000 signal Monte Carlo sample events, each containing the decay $B_s^0 \to \tau\tau$. In addition within these samples each tau is forced to decay into a 3-prong in order to have the right decay topology. In each event the neutrino masses have been minimized over one million gridpoints. No cuts have been applied and so the reconstruction efficiency on signal is $\epsilon_{reco} > 0.99$.

The histograms of two different reconstructed variables are shown in Figure 4.1. On the left hand side the deviation of the reconstructed mother decay vertex from its true value is shown on a logarithmic scale. The value filled into the histogram is

$$100 \cdot \frac{|\vec{v}_1(reco) - \vec{v}_1(true)|}{|\vec{v}_1(true)|},$$

where $v_1(reco)$ denotes the reconstructed mother decay vertex and $v_1(true)$ denotes the true decay vertex from the generator block. The mean deviation from the true vertex is 1.3 %. On the right hand side the absolute value of the difference of the true B_s^0 transverse momentum $p_\perp(true)$ and the reconstructed B_s^0 transverse momentum $p_\perp(reco)$ is displayed on a logarithmic scale. So the histogram on the right hand side is filled with the value

$$100 \cdot \frac{|p_\perp(true) - p_\perp(reco)|}{p_\perp(true)}.$$

In total roughly 1/3 of the events are reconstructed perfectly, the rest of the events are reconstructed with a not negligible error. The ambiguity in the mother decay vertex reconstruction leads to badly reconstructed events, but the number of such events decreases exponentially with the corresponding error. The tail of the distribution can be explained by the ambiguity of the solutions of the determining equations. So recapitulating it has been shown that on the generator level signal events are reconstructed to a high accuracy. This provides the desired proof of concept for the BUA reconstruction method.

4.2   Including Errors

The events used throughout the subsequent analyses are only generated, but not passed through simulation and reconstruction. By lack of time and computing power, it was not possible to fully simulate the events in CMSSW framework. In order to still have an idea of how the reconstruction algorithms will behave in a realistic setup, uncertainties on vertexing and momentum measurements were introduced: randomly generated momentum- and position vectors are added to the generated vectors. Gaussian distributions with different root mean squares (rms) where used to generate the random vectors for momenta and vertices. The widths of the gaussians in the random number generator are chosen in such a way that the resulting errors are comparable to an average contemporary particle detector. All the root mean squares applied are listed in Table 4.1.

On all momentum vectors the values that where smeared out are the pseudo-rapidity η, the polar angle ϕ and the inverse transverse momentum $1/p_\perp$. The smearing of the primary vertex was done with two different rms values for the transverse plane (xy-plane) and the beam-pipe direction z. Also for the secondary vertices two different resolutions where applied. Since the secondary vertices are reconstructed using the intersection point of reconstructed tracks, the propagation of the error of the tracks onto error of the vertex is not symmetric. The error in direction of the sum of the track momenta is bigger than the error perpendicular to this direction. This has been implemented using two different resolutions for the two components. In the study of the $B_s^0 \to \mu\tau$ decay an important input variable is the impact parameter for the muon track. The impact parameter is computed from of the primary vertex, the muon momentum and the muon production vertex. By smearing out the muon momentum and the primary vertex, the error for the impact factor is implicitly included into the data.

Moreover in all studied data samples the 3-prongs are reconstructed with the signal mass assumption. The masses of the visible particles constituting the 3-prong are all set to the π-mass at 139.57 MeV. This does not affect signal decays, but in background decays the 3-prong often contains kaons instead of pions. The mass assumption has to be implemented explicitly since after event generation all the particle masses are on their true mass. After the selection of a 3-prong all its constituting particles are set to the π-mass.

Table 4.1: The resolutions of momentum, primary- and secondary vertex.

Variable		Resolutions (rms)
Momentum	ϕ	0.58 mrad
	η	$5.8 \cdot 10^{-4}$
	$1/p_t$	$0.013 \ (\text{GeV/c})^{-1}$
Primary Vertex	xy-plane	20 μm
	z-direction	40 μm
Secondary Vertex	parallel	70 μm
	perpendicular	10 μm

4.3 Analysis of the Decay $B_s^0 \to \tau^+\tau^-$

In this section a detailed discussion and analysis of the decay $B_s^0 \to \tau\tau$ will be given. To obtain a feeling for the properties of the reconstruction without assuming a mass hypothesis, a subsection is dedicated to discuss the analysis on single decays. The goal of the discussion on single decays is, that later the analysis over many signal and background samples using the TDA method is understood on an intuitive level. The analysis over many decays is then only performed after the single event discussion. Simulated data will be presented in two different ways. On the one hand the distributions will be given on purely generated decays, where no errors are included into the data. On the other hand the distributions will also be given on decays where errors are included using gaussian distributions as explained in the previous section. A complete and formal discussion of the applied reconstruction algorithm is given in Section 3.3.3.

4.3.1 The processing of Single Decays

It is obvious that in order to interpret the results obtained with a reconstruction algorithm, understanding the processing of single events is important. In the present case, this is not a trivial task since even for single events the reconstruction can not be done analytically. Here the single event processing is discussed on one explicit example. As it was shown, the physics part of the reconstruction formally provides an one-dimensional set of possible solutions. So for each event to be reconstructed, there is a continuous set of possibilities for the reconstruction of the event. For each observed final state of the assumed decay topology, there is an infinite number of events that could have led to this final state. An example of such a set is shown in figure 4.2. The figure shows a special parametrisation for the area within the triangle of possible decay vertices. This area scanned for possible decay vertices has been parametrised by x and y such that $(x, y) \in [0, 1] \times [0, 1]$. Let v_2 and v_3 be the decay vertices of the tau leptons. Then the parametrisation of the B_s^0 decay vertex
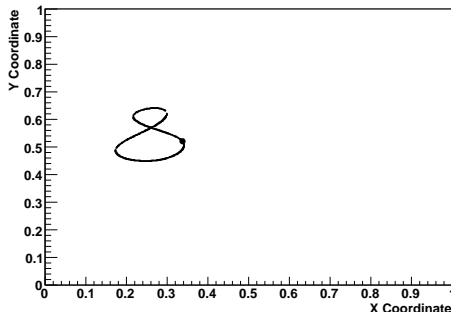
Figure 4.2: The set of solutions for a single $B_s^0 \to \tau^+\tau^-$ event in normalized coordinates. The black dot marks the true decay vertex position.

v_1 is defined as follows:

$$v_1(x, y) = x \cdot \big(v_2 + y \cdot (v_3 - v_2)\big).$$

Within this parametrisation the coordinates of roughly 30'000 convergence points are drawn in Figure 4.2. The convergence points are obtained by looking for good starting points[2] and running a Migrad minimization from these starting points. The good starting points where selected out of 250000 tested starting points. Whenever migrad converged from one of the good starting points, the computed convergence point was filled into the histogram. Along the marked line in the histogram, the reconstructed τ-momenta are numerically balanced with respect to the corresponding B_s^0 flight direction. A priori there exists no discriminating variable that allows to choose any particular vertex out of these possibilities. Still there is one useful and simple property of this set in each event: it always contains the true reconstruction vertex. In order to understand how this can be used, recall that the set of possible mother decay vertices is obtained by balancing the momenta of the reconstructed τ-leptons with respect to a corresponding mother flight direction. For each vertex which has the reconstructed τ-momenta balanced, a two body decay could have happened at that vertex. The invariant mass of the reconstructed mother particle is the invariant mass of the system of the two τ-leptons. Since the set of solutions is continuous, in a small neighborhood around the true decay vertex, the masses will be in a small neighborhood of the true invariant mass of the mother particle. Therefore it is clear that information about the true initial mass of the mother particle is contained in the set of solutions. The minimization of the critical value (the balancing of the tau momenta) is then somewhat arbitrary since formally none of the points along the given curve of one event is distinguishable from the others.

---

[2]as defined in Section 3.3.3

But since the true vertex and the corresponding mass are also located on the curve, when plotting the values of many events, the mass of the particle can still be reconstructed. The results that can be obtained with this methods are presented in the next section.

The reconstruction of the tau momenta is done applying the NR, and so for each tau there are two possible reconstructed momenta leaving a two fold ambiguity. Since for the reconstruction of the whole decay the reconstructed tau momenta have to be combined, both two fold ambiguities together provide four different combinations for each possible decay vertex. As explained in Section 3.3.1 the two solutions for each tau can formally be ordered according to high- and low momentum[3]. Therefore the four combinations will be ordered according to the total energy of the reconstructed B_s^0. Since the solutions depend continuously on the parametrisation variables x and y, it is then clear that the four different combinations can be treated separately within each event. Each combination provides its own continuous subset of possible decay vertices. However in most cases, the sets together also form a connected curve. This can also be seen in Figure 4.2 where all combinations are plotted in the same histogram. Some more details about the properties of the one-dimensional set of mother decay vertices in each single decay, which are not relevant here, are discussed in Appendix B.

Before going from one event to many events, there is one additional obstacle to overcome: it is not possible to store all the convergence points of the Migrad algorithm. It is necessary to choose a manageable number of convergence points per event. But the number of convergence points depends only on the number of starting points and how those starting points are distributed within the scan area. It can be arbitrarily changed by the experimentator. The more starting points are used, the more convergence points are found. A higher number of convergence points only results in a better resolution along the one-dimensional set of solutions. So it becomes clear that the criteria to choose some of these points are a crucial ingredient to the reconstruction algorithm. As mentioned several times before, there are four separate subsets of the overall solutions. These appear due to the ambiguities in the neutrino reconstruction method which is applied twice. They can be distinguished because the four combinations differ by the decay direction of the 3-prongs in each tau decay. So since the momenta of the reconstructed particles are different for the four combinations, only one of the subsets contains the true decay vertex. This separation suggests a first criterion for the selection of convergence point: in each event at most four convergence points are stored, one for each combination. Note that depending on the decay it is possible that some of the combinations may not provide any convergence point and thus not in every decay there are four vertices stored. Of course the criterion that is applied to choose the convergence point within one combination is the same for all four combinations.

At each convergence point a B_s^0 candidate can be reconstructed. The mass of the B_s^0 candidate varies for different decay vertices but matches the true B_s^0 mass at

---

[3]or equivalently according to forward- and backward decay of the 3-prong

the true decay vertex. However this mass is not assumed and thus the true decay vertex can not be singled out. To choose a mother decay vertex within one combination, the average mass over all convergence points is computed. In order to obtain an unbiased average of the mass distribution, a numerical weighting of the convergence points has to be avoided. This is done by segmenting the scan area and marking each segment containing at least one convergence point. A segment containing many convergence point is treated in the same way as a segment with only one convergence point. The average mass is then computed with the masses of the segments. Finally the segment which corresponds to the mass which is closest to the average is selected as the final reconstruction vertex.

4.3.2   Event Simulation

The analysis of the decay $B_s^0 \to \tau^+\tau^-$ is done using three different sets of generated Monte Carlo samples: a signal, a resonant background and a generic background sample. The resonant background sample is chosen as an example for the behavior of the algorithm on resonant background. In all samples the events have been generated only with gluon-gluon fusion. The b-quarks are forced to be separated in pseudo-rapidity η via the following settings in Pythia:

```
'CKIN(13)=0.0 !  etamin'
'CKIN(14)=2.5 !  etamax'
'CKIN(15)=-2.5 !  -etamax'
'CKIN(16)=0.0 !  -etamin'.
```

With this settings it is assumed that the gluon-gluon fusion cross section can be scaled up according to the expected contributions from gluon splitting and from flavor excitation. The total $b\bar{b}$-production cross section $\sigma_{gen}^{b\bar{b}}$ is assumed to be 480 μb. In the signal sample and in the resonant background sample both b-quarks are forced to fragmentate into a B_s^0 meson. The resonant background sample contains $B_s^0 \to D^+D^-$ decays where both $D^\pm$ mesons decay $D^+ \to e^+\pi^-K^+\nu_e$. The generic background sample contains unbiased $b\bar{b}$-events. Table 4.2 summarizes the properties of the generated the event samples. The lo-$b\bar{b}$ stands for the leading order Pythia production and the constraints on the b-quarks which where applied. The visible luminosities are defined by

$$\mathcal{L}_{vis} = \frac{N_{Gen}}{\sigma_{gen}^{b\bar{b}} \cdot \epsilon_{gcuts} \cdot 2\,f_s \cdot \mathcal{B}} \;,$$

where N_{Gen} is the number of generated events, ϵ_{gcuts} is the efficiency of the cuts in Pythia, f_s is the fragmentation ratio $b \to s$ and $\mathcal{B}$ is the total branching fraction of all the forced decays in the different samples. The production cross sections in Table 4.2 are defined by $\sigma_{prod} = \sigma_{gen}^{b\bar{b}} \cdot \epsilon_{gcuts}$. The branching ratios which where assumed to compute the cross sections and integrated luminosities are listed in Table 4.3. Note

Table 4.2: Event samples used in the analysis of $B_s^0 \to \tau^+\tau^-$. The cuts on generator level, the generated number of events, the production cross sections and the corresponding integrated luminosity are given. All samples are from private production.

SAMPLE	GENERATOR CUTS	N_{Gen}	σ_{prod} [mb]	$\mathcal{L}_{vis}$ [fb^{-1}]
Signal	$\left|\eta^b\right| < 2.5$, lo-$b\bar{b}$	234228	1.1×10^{-1}	3.6×10^{2}
Res. bg.	$\left|\eta^b\right| < 2.5$, lo-$b\bar{b}$	223030	1.1×10^{-1}	1.0×10^{2}
Gen. $b\bar{b}$ bg.	$\left|\eta^b\right| < 2.5$, lo-$b\bar{b}$	5.0×10^{6}	4.8×10^{-1}	1.0×10^{-5}

Table 4.3: Branching Ratios (BR) for the forced decays in the private Monte Carlo production.

DECAY CHANNEL	BR	SOURCE
$B_s \to \tau^+\tau^-$	7.31×10^{-7}	[8], [9]
$\tau^- \to \pi^-\pi^+\pi^-\nu_\tau$	8.99×10^{-2}	[15]
$B_s \to D^+D^-$	1×10^{-5}	[15]
$D^+ \to e^+(K^-\pi^+)\nu_e$	4.5×10^{-2}	[15]

that the branching ratio for the decay $B_s^0 \to D^+D^-$ has not yet been measured. Therefore it is estimated by the $B_c^0 \to \overline{D^0}\pi^0$ branching ratio where the two decays are assumed to differ only in the spectator quark. So the B_c^0 decay is assumed to equal the B_s^0 decay up to a Cabibbo suppression by a factor of $|V_{cs}/V_{ud}|^2 \sim 0.05$.

4.3.3 3-Prong Selection

The selection of the decays within the generated events is done by looking for 3-prongs. A 3-prong is defined as three detectable, charged and stable particles originating from the same vertex. Effectively the 3-prong candidates are selected by the following requirements:

1. The production vertices of the selected particles have to be in the same sphere with radius $\epsilon < 10^{-9}$ mm and separated at least 20 μm from the primary vertex.

2. All selected particles have to be stable.

3. Among all selected particles which are detectable there are exactly three satisfying $|\eta| < 2.5$ and $p_\perp > 0.5$ GeV. Moreover the sum of their charges has to be ± 1.

Whenever for a set of particles the above requirements are satisfied, the set is stored as a 3-prong candidate. Since in each 3-prong all the constituting particles have to

Table 4.4: Reconstruction efficiencies for the different Monte Carlo event samples.

SAMPLE	EFFICIENCY TRUTH	EFFICIENCY SMEARED
Signal	5.18×10^{-1}	2.58×10^{-1}
Res. Background	5.27×10^{-1}	4.20×10^{-1}
Background	3.78×10^{-1}	3.09×10^{-1}

pass kinematic cuts, in the same event only rarely more than two 3-prongs survived the selection criteria. If nevertheless within an event there are more than two 3-prongs left after the selection, the angle between the visible 3-prong momentum and its vertex is computed. Those two 3-prongs with the smallest such angles are kept as candidates for the reconstruction. The 3-prong multiplicity is displayed in Figure C.4. In some cases the selection criteria presented here lead to a wrong selection of the 3-prongs. In the signal histogram in Figure 4.4 the entries with large angles between the reconstructed τ-momenta are due to this wrong selections.

4.3.4   Analysis

An analysis of the decay $B_s^0 \to \tau^+\tau^-$ can now be made straightforward. The TDA reconstruction algorithm is run on the three generated sets of events: the signal sample, the resonant background sample and the generic background sample. The properties of the different samples are discussed in Section 4.3.2. The distributions of the reconstructed B_s^0-candidate mass for the different samples are shown in Figure 4.3. Note that here only the most relevant distributions will be shown, for additional plots see Appendix C.

The reconstruction efficiencies for the reconstruction with smeared respectively with unsmeared variables are given in Table 4.4. The reconstruction efficiency with smeared variables is higher on background than on signal. For the resonant background the reason for this could be is the lifetime of the $D^{\pm}$-meson which leads to a larger area with possible positions of the B_s^0 decay vertex. The lifetime of the $D^{\pm}$-meson is more than three times larger than the lifetime of the τ-lepton. A larger area also leads to more possible reconstruction vertices. For the generic background similar considerations apply.

Resolution on Signal

The resolutions obtained with the TDA method are shown in Figure 4.3. In the histograms there are roughly four entries per decay since the all the solutions from the different combinations are included[4]. The most important quantities are the mass distributions in Figure 4.3, where the mass of the reconstructed B_s^0 is displayed once for purely generated decays and once for decays with errors included. The mass

---

[4]recall that the application of the NR most often leads to four solutions per event

resolutions for purely generated events is 700 MeV whereas in a realistic set up a mass resolution of roughly 900 MeV can be expected. Since for each decay there is a big combinatorial background, the mass resolution is quite limited even without errors. The resolutions on the B_s^0 transverse momentum and the transverse momenta of the two reconstructed τ-leptons are also given in Figure 4.3 on a logarithmic scale. Both plots show the deviation of the reconstructed values from the true values in %. For these plots the reconstruction has been performed on the unsmeared variables to show only the influence of the combinatorial background on the reconstruction. The introduction of errors on the selected variables has a smaller effect on the resolutions than the combinatorial background.

Distributions and Cuts

The cut variables and distributions needed to obtain the final results are presented here. The most important distributions are given for all three generated events samples. In Figure 4.5 the distributions of the visible variables are shown: transverse momenta of the selected 3-prongs and the length of the corresponding τ decay vertices. In Figure 4.6 the distributions of two reconstructed variables are shown: the transverse momenta of the τ-leptons and the B_s^0. The distributions do not differ strongly for the signal samples and for the background samples, so in order to separate signal from background some other variables are needed. The variables which where used as cut variables are the B_s^0-mass and the three following variables

$$
\begin{aligned}
\psi_{pp} &= \arccos\left(\frac{\vec{p}_1 \cdot \vec{p}_2}{|\vec{p}_1|\,|\vec{p}_2|}\right), \\
\psi_{vv} &= \arccos\left(\frac{\vec{v}_1 \cdot \vec{v}_2}{|\vec{v}_1|\,|\vec{v}_2|}\right), \\
\Delta V &= \big|\,|\vec{v}_1| - |\vec{v}_2|\,\big|,
\end{aligned}
$$

where $p_{1,2}$ are the reconstructed τ-momenta and $v_{1,2}$ are the τ-decay vertices. So the cut variables are the angle between the two 3-prong momenta ψ_{pp} (PPAngle), the angle between the reconstructed τ-momenta ψ_{vv} (VVAngle) and the length distance between the two selected τ-vertices ΔV (LDiff). What will be referred to as the length of a vertex is defined as the distance of the vertex to the primary vertex. Figure 4.4 displays the distributions for the cut variables. The lower and upper bounds for the cut variables are summarized in Table 4.5 and also marked with vertical lines in Figure 4.4.
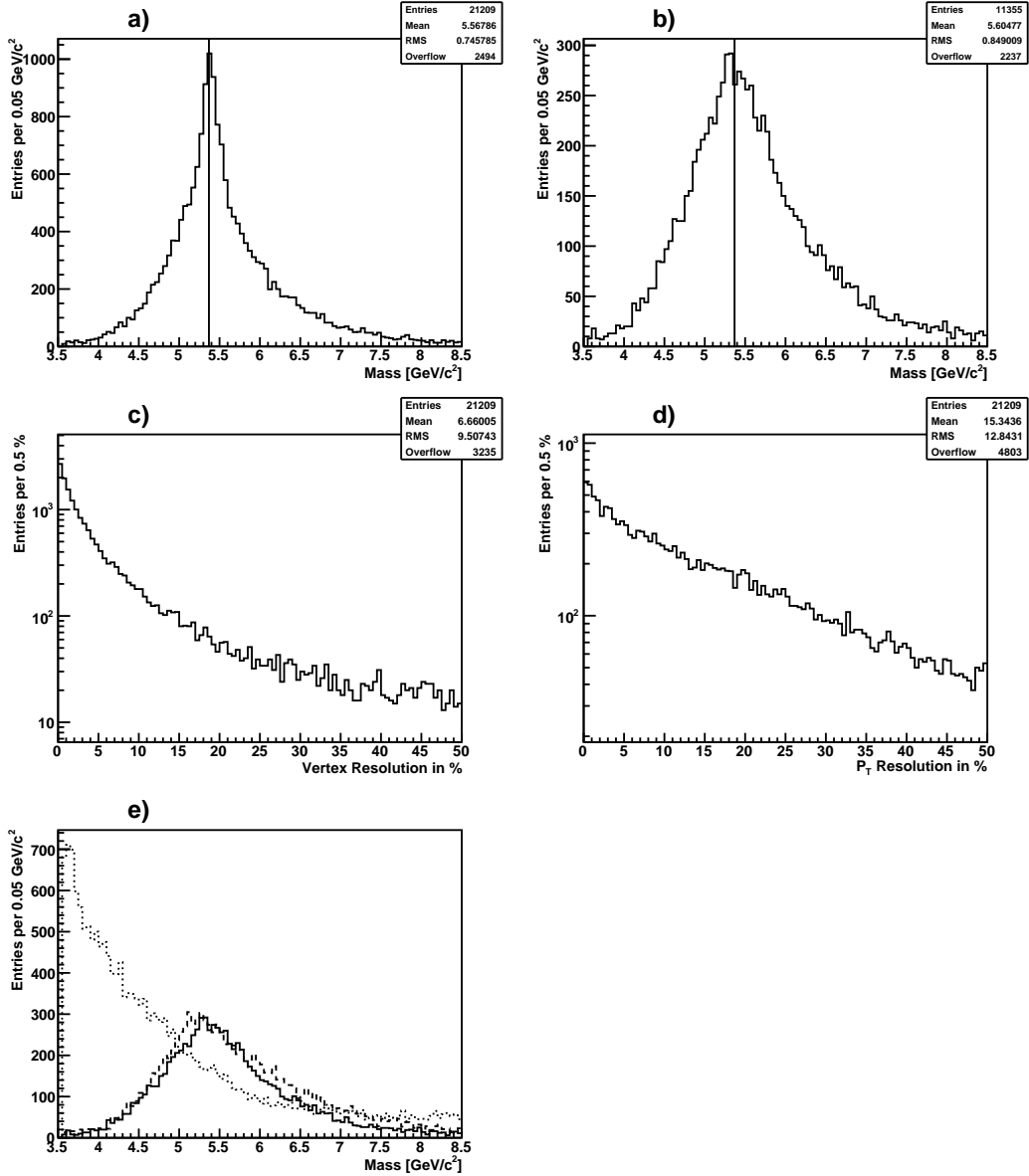
Figure 4.3: Distributions of the reconstructed B_s^0-candidate mass: a) before smearing, b) after smearing. The vertical line is located at the true B_s^0-mass of 5.369 GeV. The resolutions for two reconstructed B_s^0-candidate variables in a logarithmic scale are shown: c) vertex, d) transverse momentum. In e) the mass distributions for the three event samples are shown: signal (full line), resonant background (dashed line) and generic background (dotted line).
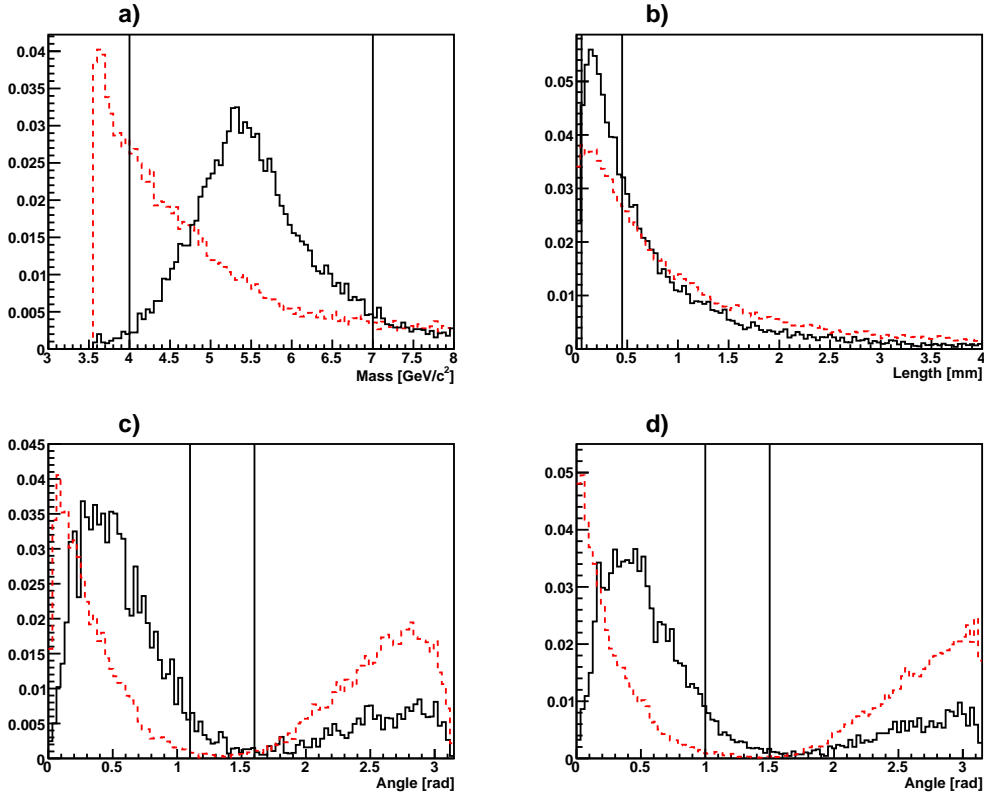
Figure 4.4: The distributions of the cut variables: a) Reconstructed B_s^0-candidate Mass, b) length difference between the two τ decay vertices, c) angle between the reconstructed τ-momenta, d) angle between the two 3-prong momenta. The vertical lines indicate the low respectively the high cut on the variables. The full line shows the signal distributions, the dashed lines display the background distributions. All histograms are normalized to equal area.

Table 4.5: Lower and upper bounds for the cut variables.

CUT VARIABLE		BOUNDS
B_s^0-Mass	[GeV]	$4 < m_B < 7$
PPAngle	[rad]	$1.1 < \psi_{pp} < 1.6$
VVAngle	[rad]	$1.0 < \psi_{vv} < 1.5$
LDiff.	[mm]	$0.05 < \Delta V < 0.45$
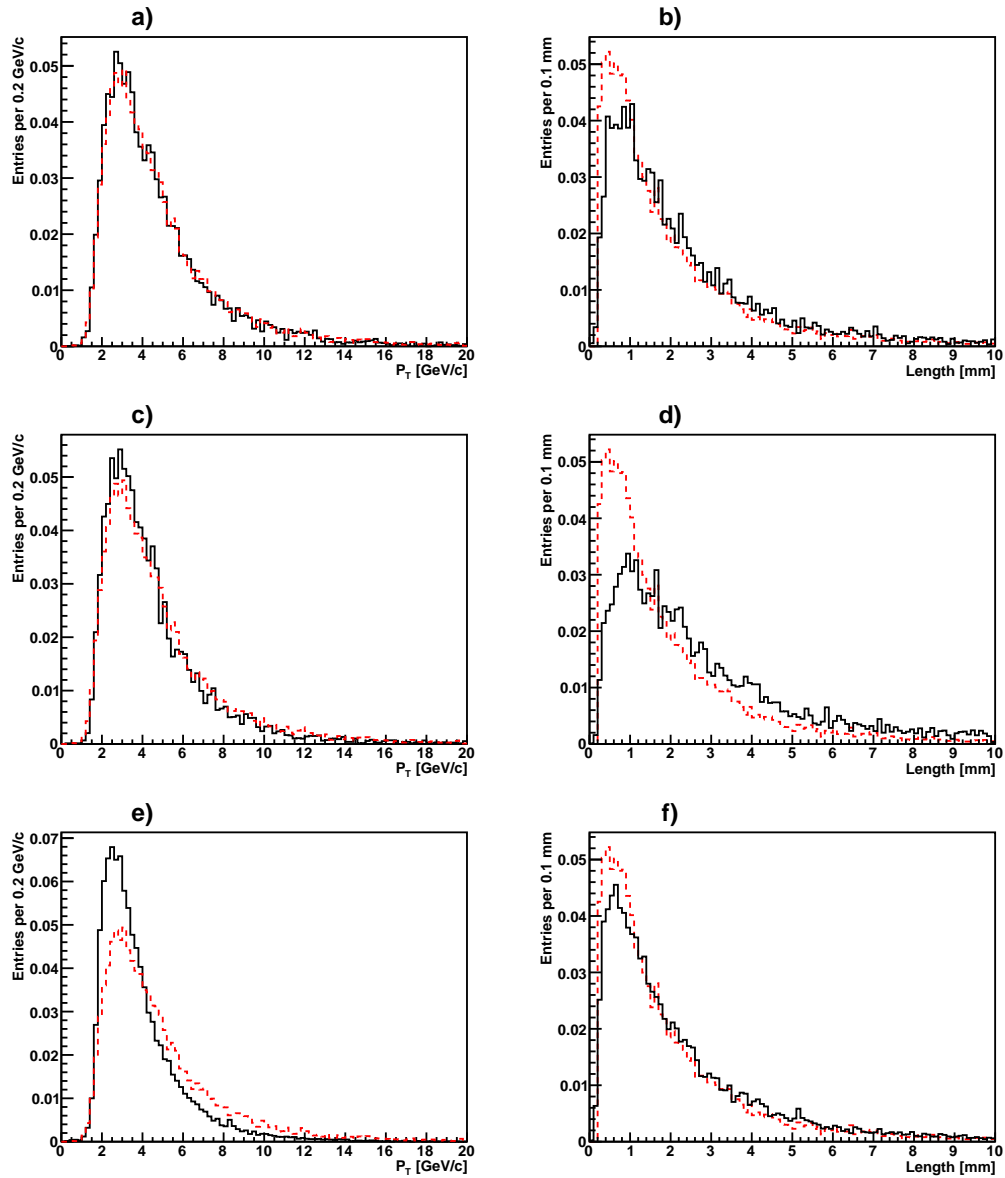
Figure 4.5: The smeared 3-prong transverse momenta are shown in a) for signal, in c) for resonant background and in e) for generic background. The length of the displaced decay vertices of the τ-leptons are shown in b) for signal, in d) for resonant background and in f) for generic background. For comparison in all plots the dashed histogram shows the unsmeared signal distribution of the corresponding value. The histograms are normalized to equal area.
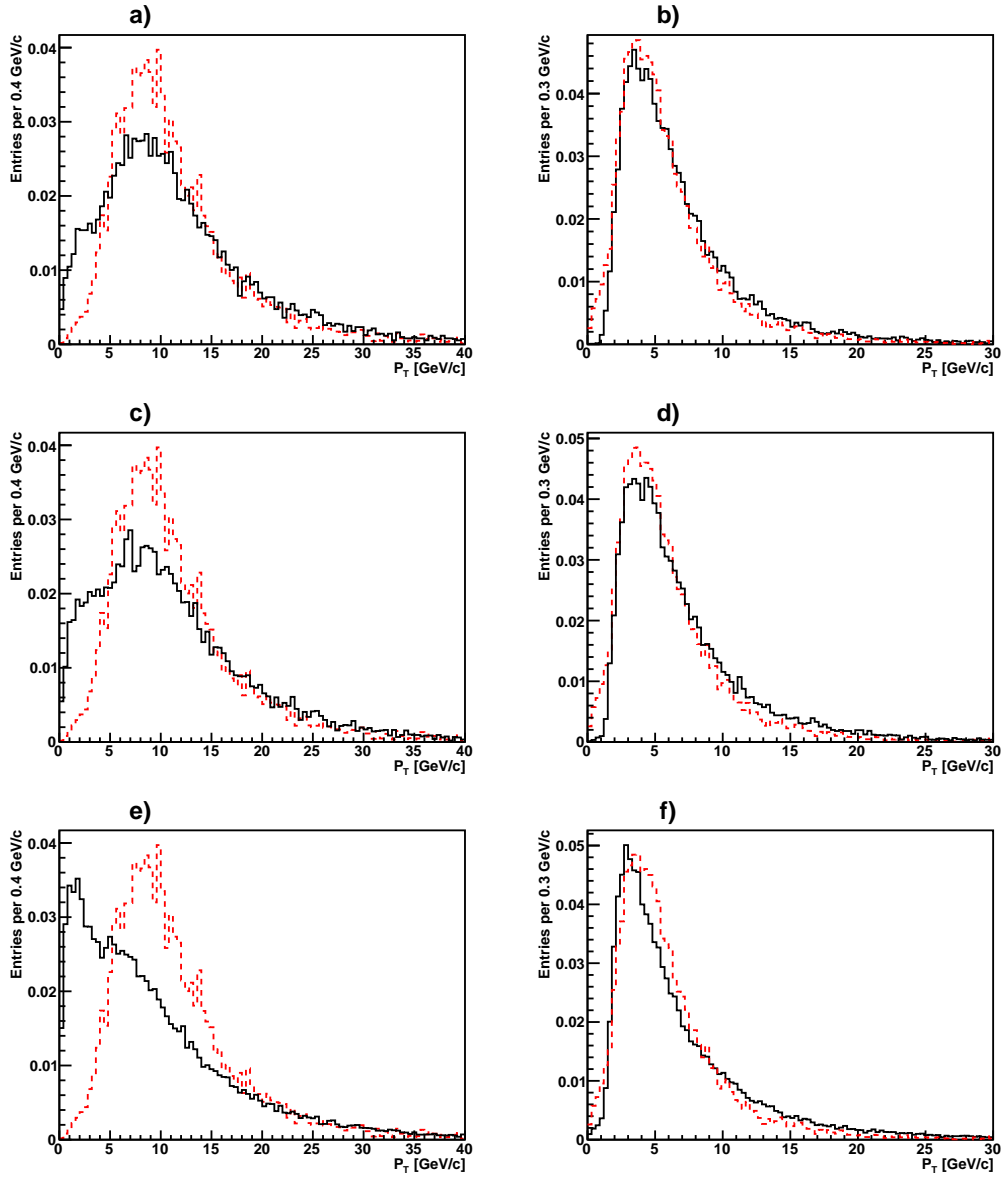
Figure 4.6: The reconstructed B_s^0-candidate transverse momentum is shown in a) for signal, in c) for resonant background and in e) for generic background. The reconstructed transverse momenta of the τ-leptons are shown in b) for signal, in d) for resonant background and in f) for generic background. For comparison in all plots the dashed histogram shows the unsmeared signal distribution of the corresponding value. The histograms are normalized to equal area.

4.3.5   Results

After applying all the cuts 89 signal and 11 background decays remain in the given mass window, which correspond to total efficiencies of $\epsilon_{\text{Total}} = 3.8 \times 10^{-4}$ for signal and $\epsilon_{\text{Total}} = 4.9 \times 10^{-5}$ for background. The normalization to 1 fb^{-1} of the two samples with the assumed branching ratios leads to a scaling factor of 2.3×10^{-3} for the signal events and 9.6×10^{4} for the background events. So a discovery of the decay is out of reach even for substantially higher integrated luminosities. Only an upper limit on the signal branching ratio can be given. The upper limit corresponds to the signal branching fraction at which a 2σ discovery of the decay can be achieved. The resulting expected upper bound for a data sample of 1 fb^{-1} is

$$\mathcal{B}(B_s^0 \to \tau^+\tau^-) < 6.2 \times 10^{-3},$$

at the 95% confidence level. The calculation of the upper bound presented here is given in Appendix A. Note that this upper bound only gives a very rough estimation of the possibilities that the presented method to reconstruct such decays provide. The branching ratio has only limited validity due to the subsequent reasons: in the present analysis the trigger issue has been left away completely. At hadron colliders this is a strong limitation on the validity of the expected upper bound presented here, since the efficiency on the selection level would decrease substantially when trigger cuts where applied. Moreover Pythia relies only on leading order calculations. The assumption that the Pythia Monte Carlo samples generated only with gluon-gluon fusion can be scaled up to the full $b\bar{b}$ production cross section should be remembered. Also the decay of the τ-leptons is not implemented properly in the Pythia event generator. So it is clear that the upper bound presented here should be considered critically.

4.4   Analysis of the Decay $B_s^0 \to \mu^\pm \tau^\mp$

In this section a detailed discussion and analysis of the decay $B_s^0 \to \mu^\pm\tau^\mp$ will be given. Also here simulated data will be presented before and after introducing errors. The details of the reconstruction are described in Section 3.3.4. The handling of single events is described there and only one technical detail is left which has still to be mentioned. Since the whole analysis is performed on purely generated events, there are no track objects stored in the data. For the $B_s^0 \to \tau^+\tau^-$ analysis the objects needed for the reconstruction are the same as those which are obtained after a full detector simulation and the introducing of the error by hand can be done straightforward. But for the $B_s^0 \to \mu^\pm\tau^\mp$ analysis, a variable is needed which is only produced in a detector simulation: the impact parameter. So the impact parameter has to be explicitly computed using the B_s^0 decay vertex and the direction of the muon momentum. This is done by means of the following formula

$$\vec{v}_{impact} = \vec{v}_1 - \left(\frac{\vec{v}_1 \cdot \vec{p}_\mu}{|\vec{p}_\mu|^2} \right) \cdot \vec{p}_\mu,$$

Table 4.6: Event samples used in the analysis of $B_s^0 \to \mu^\pm \tau^\mp$. The cuts on generator level, the generated number of events, the production cross section and the corresponding integrated luminosity are given. All samples are from private production.

SAMPLE	GENERATOR CUTS	N_{Gen}	σ_{prod} [mb]	$\mathcal{L}_{vis}$ [fb^{-1}]
Signal	$\left|\eta^b\right| < 2.5$, lo-$b\bar{b}$	446493	1.1×10^{-1}	-
Gen. $b\bar{b}$ bg.	$\left|\eta^b\right| < 2.5$, lo-$b\bar{b}$	44773	6.7×10^{-4}	6.7×10^{-5}
	$\left|\eta_\mu\right| < 2.5$, $p_{\perp,\mu} > 3$ GeV			
	$\left|\eta_h\right| < 2.5$, $p_{\perp,h} > 3$ GeV			

where $\vec{v}_{impact}$ is the impact parameter, $\vec{p}_\mu$ is the muon momentum and $\vec{v}_1$ is the mother decay vertex. The impact parameter will be computed for each decay. The smearing of the impact parameter is then implicitly done in its reconstruction. After including errors, the impact parameter is computed with the smeared muon momentum and the displaced primary vertex and so their error automatically propagates on to the impact parameter.

4.4.1 Event Simulation

For the decay $B_s^0 \to \mu^\pm \tau^\mp$ two different samples where produced with the Pythia Monte Carlo event generator. A signal sample and a generic background sample. The production settings are the same as in Section 4.3.2, but with different forced decays. In the signal sample the decay $B_s^0 \to \mu^\pm \tau^\mp$ is forced, in the generic background no decays where forced but some strong kinematical constraints where applied. The cuts on generator level and the other properties of the event samples are displayed in Table 4.6. The production cross sections and the corresponding integrated luminosities have the same definitions as in Section 4.3.2. The index h stands for the hadronic system. For the signal sample no assumption was made about the branching ratio of $B_s^0 \to \mu^\pm \tau^\mp$ and therefore no corresponding integrated luminosity is assigned to the sample.

4.4.2 3-Prong and Muon Selection

The selection of 3-prongs in the events is done similar to the selection in Section 4.3.3. In addition to select a the 3-prong in each event, also μ-candidates have to be selected. If more than one μ-lepton is found in an event, the μ-candidate with the highest transverse momentum is kept for reconstruction. The 3-prong multiplicity is low because of the kinematical cuts on the particles constituting the 3-prong. When anyhow more than one 3-prong is found, the angle between the 3-prong momentum and the μ-candidate is computed and the 3-prong which is closest to the μ-candidate is kept for reconstruction. The 3-prong and the μ multiplicity in each event is shown in Figure D.5.

Table 4.7: Reconstruction efficiencies for the different Monte Carlo event samples.

SAMPLE	EFFICIENCY TRUTH	EFFICIENCY SMEARED
Signal	6.78×10^{-1}	3.68×10^{-1}
Background	4.69×10^{-2}	1.2×10^{-1}

4.4.3   Analysis

An analysis of the decay $B_s^0 \rightarrow \mu^{\pm} + \tau^{\mp}$ can now be made straightforward. The TDL reconstruction algorithm is run on the two generated sets of events: the signal sample and the generic background sample. The properties of the different samples are discussed in Section 4.4.1. Note that here only the most relevant distributions will be shown, for additional plots see Appendix D. The reconstruction efficiencies for the reconstruction with smeared respectively with unsmeared variables are given in Table 4.7.

Resolution on Signal

The resolutions obtained with the TDL method are shown in Figure 4.7. The most important quantities are the mass distributions in Figure 4.7, where the mass of the reconstructed B_s^0 is displayed once for purely generated decays and once for decays with errors included. Most often there are two reconstructed masses per event, but one of the two solutions will always be on the true B_s^0-mass of 5.369 GeV. The mass resolution for purely generated events is very narrow and can be considered as only numerically limited. In a realistic set up a mass distribution gets broadened and the with remains at roughly 700 MeV. The resolutions on the B_s^0 transverse momentum and the transverse momenta of the two reconstructed τ-leptons are given in Figure 4.7 on a logarithmic scale. Both plots show the deviation of the reconstructed values from the true values in %. For these plots the reconstruction has been performed on the unsmeared variables to show only the influence of the combinatorial background on the reconstruction. For most events there are two entries and one of the entries has the true coordinates and the correct transverse momentum of the τ-lepton.

Distributions and Cuts

The cut variables needed to obtain the final results and some basic distributions are presented here. The distributions are given for both generated events samples. In Figure 4.9 the distributions of three visible variables are shown: the transverse momentum of the 3-prong, the transverse momentum of the μ-lepton and the length of the τ-decay vertex. In Figure 4.10 the distributions of three reconstructed variables are shown: the transverse momentum of the τ-lepton, the transverse momentum of the B_s^0 and the length of the B_s^0-decay vertex. The distributions do not differ strongly for the signal samples and for the background samples, so in order to sep-
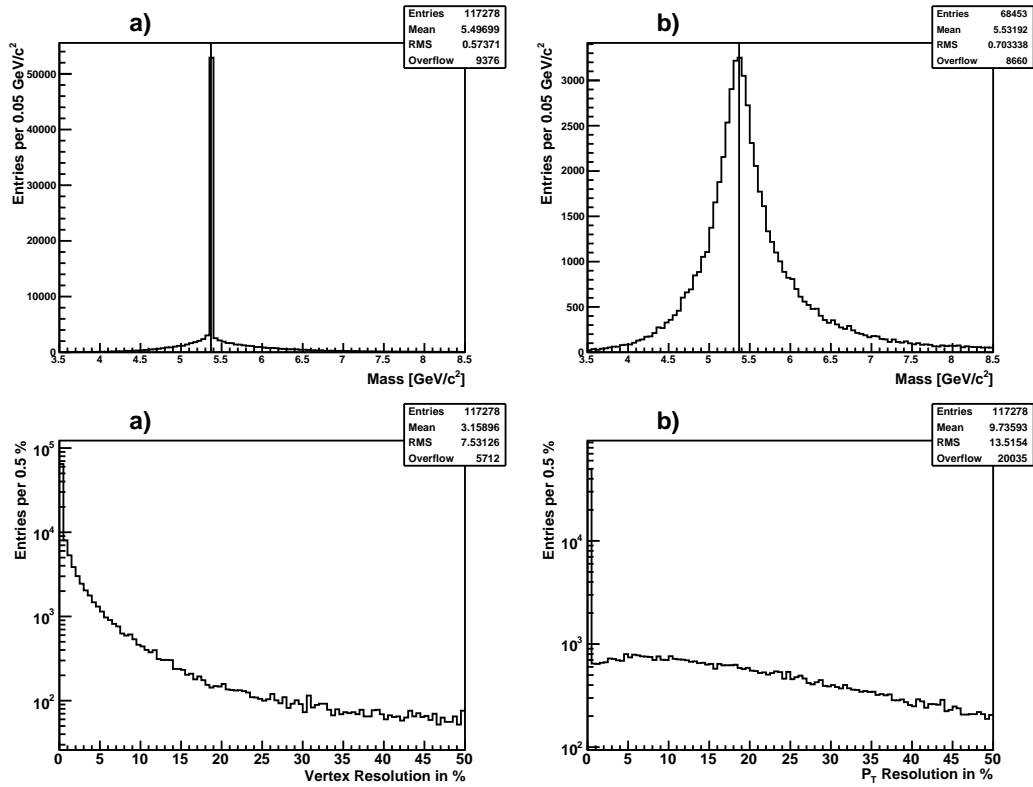
Figure 4.7: Distributions of the reconstructed B_s^0-candidate mass: a) before smearing, b) after smearing. The vertical line is located at the true B_s^0-mass of 5.369 GeV. The Resolutions for two reconstructed B_s^0-variables in a logarithmic scale: a) vertex, b) transverse momentum
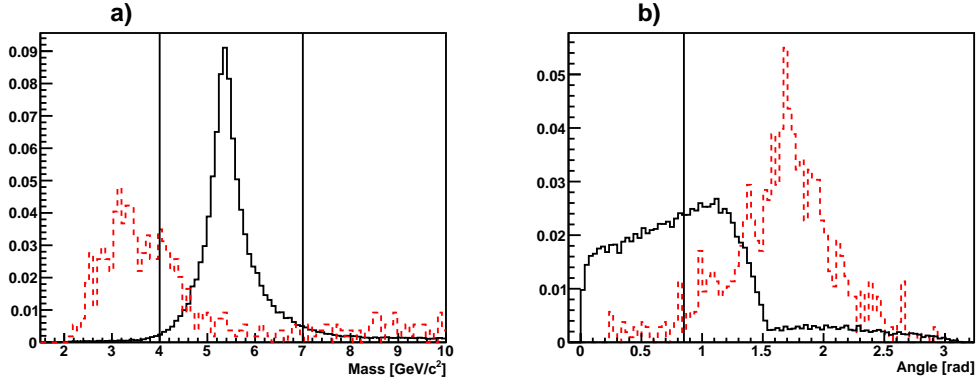
Figure 4.8: The distributions of the cut variables: a) Reconstructed B_s^0-candidate Mass, b) the angle between the impact parameter and the τ-decay vertex. In a) the vertical lines indicate the low respectively the high cut on the variables. In b) there is only a high cut at the vertical line. In all histograms the full line shows the signal distributions, the dashed lines display the background distributions. The histograms are normalized to equal area.

Table 4.8: Lower and upper bounds for the cut variables.

CUT VARIABLE		BOUNDS
B_s^0-Mass	[GeV]	$4 < m_B < 7$
IPVAngle	[rad]	$0 < \psi_{cut} < 0.85$

arate signal from background some other variables are needed. Figure 4.8 displays the distributions for the cut variables. The cut variables are the B_s^0 mass and the angle between the impact parameter and the τ-decay vertex ψ_{cut} (IPVAngle). This angle is defined as follows

$$\psi_{cut} = \arccos \left(\frac{|\vec{v}_I \cdot \vec{v}_\tau|}{|\vec{v}_I|\,|\vec{v}_\tau|} \right),$$

where v_I denotes the impact parameter and v_τ denotes the τ-decay vertex. The lower and upper bounds for the cut variables are summarized in Table 4.8 and also marked with vertical lines in Figure 4.8.

4.4.4   Results

After applying all the cuts 17506 signal and 0 background decays remain in the given mass window, which correspond to total efficiencies of $\epsilon_{\text{Total}} = 3.8 \times 10^{-2}$ for signal and $\epsilon_{\text{Total}} \sim 0$ for background. The normalization of the background sample to 1
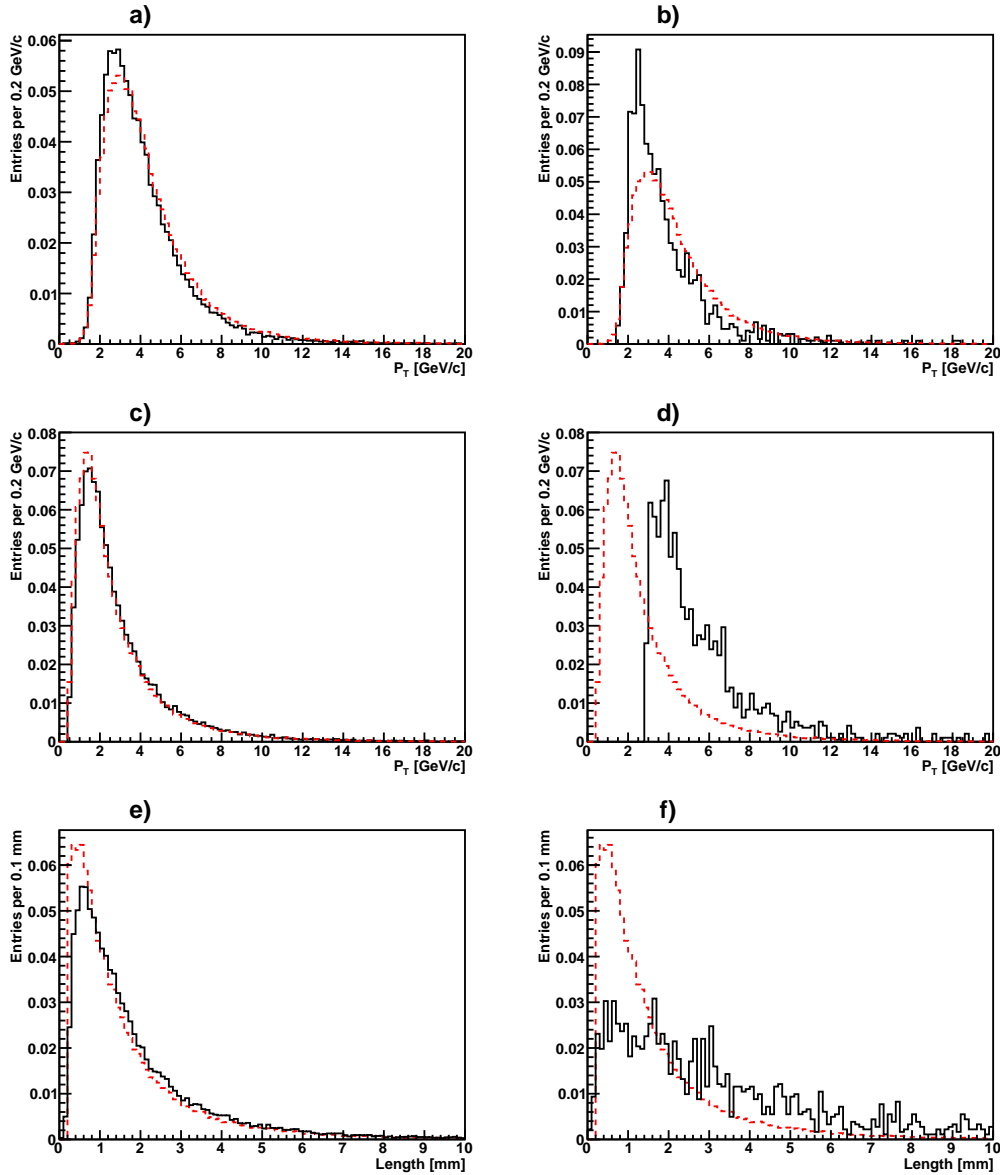
Figure 4.9: The smeared 3-prong transverse momentum is shown in a) for signal and in b) background. The smeared transverse momentum of the muon is shown in c) for signal and in d) for background. The length of the τ-decay vertex is shown in e) for signal and in f) background. For comparison in all plots the dashed histogram shows the unsmeared signal distribution of the corresponding value. The histograms are normalized to equal area.
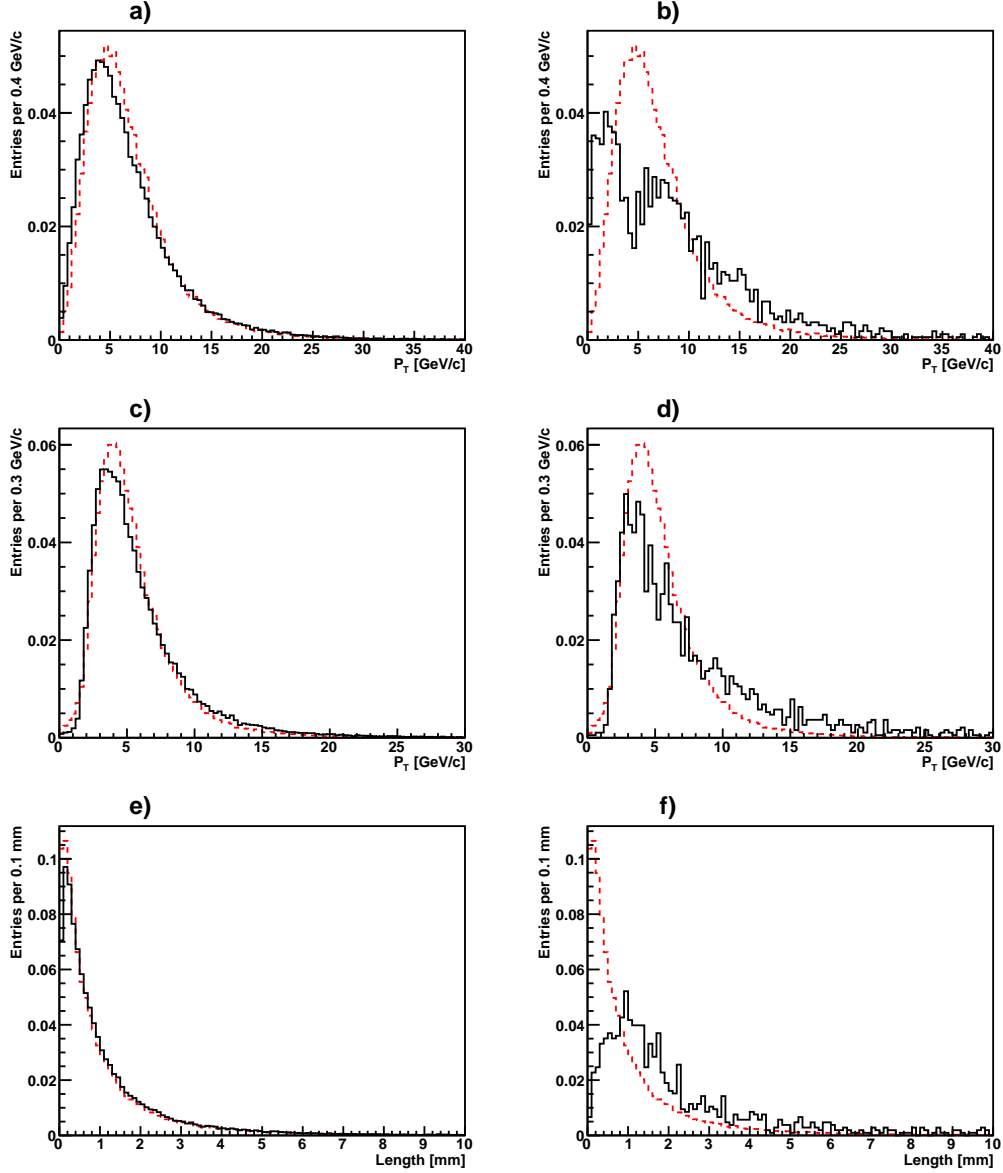
Figure 4.10: The reconstructed B_s^0-candidate transverse momentum is shown in a) for signal and in b) for background. The reconstructed transverse momenta of the τ-lepton is shown in c) for signal and in d) background. The length of the reconstructed B_s^0-candidate vertex is shown in e) for signal and in f) for background. For comparison in all plots the dashed histogram shows the unsmeared signal distribution of the corresponding value. The histograms are normalized to equal area.

fb^{-1} with the assumed branching ratio leads to a scaling factor of 1.5×10^4 for the background events. An upper limit on the signal branching ratio will be given. The upper limit corresponds to the signal branching fraction at which a 2σ discovery of the decay can be achieved. The resulting expected upper bound for a data sample of 1 fb^{-1} is

$$\mathcal{B}(B_s^0 \rightarrow \mu^{\pm}\tau^{\mp}) < 1.9 \times 10^{-6},$$

at the 95% confidence level. The calculation of the upper bound presented here is given in Appendix A. Note that this upper bound only gives a very rough estimation of the possibilities that the presented method to reconstruct such decays provide. The branching ratio has only limited validity due to the subsequent reasons: in the present analysis the trigger issue has been left away completely. At hadron colliders this is a strong limitation on the validity of the expected upper bound presented here, since the efficiency on the selection level would decrease substantially when trigger cuts where applied. Moreover Pythia relies only on leading order calculations. The assumption that the Pythia Monte Carlo samples generated only with gluon-gluon fusion can be scaled up to the full $b\bar{b}$ production cross section should be remembered. Also the decay of the τ-leptons is not implemented properly in the Pythia event generator. So it is clear that the upper bound presented here should be considered critically.

Chapter 5

Conclusions and Outlook

Three reconstruction methods have been presented. The methods provide a possibility to reconstruct decays containing missing particles by using topological information. This has been shown by applying the methods to the decays $B_s^0 \to \tau^+\tau^-$ and $B_s^0 \to \mu^\pm\tau^\mp$, where the τ-leptons in both decays are assumed to decay in a 3-prong. The topological information needed to reconstruct the decays successfully are the two decay vertices of the τ-leptons. By assuming the 3-prong decay channel for the τ-leptons it becomes possible to reconstruct these vertices using the 3-prong tracks. The two decays that have been studied are good examples for the decay topologies that can be reconstructed with the methods.

The first method reconstructs the decay $B_s^0 \to \tau^+\tau^-$ assuming the mass of the B_s^0 meson and has only been applied superficially to make a proof of concept. The second reconstruction method reconstructs the same decay without assuming the mass of the B_s^0 meson. With this method an analysis of the decay has been performed on simulated data. It has been shown that a mass resolution of about 900 MeV should be achievable in an average collider experiment. The third reconstruction method reconstructs the decay $B_s^0 \to \mu^\pm\tau^\mp$. Also for this decay an analysis has been made and the mass resolution that can be expected from this method in a realistic experimental environment is 700 MeV.

The analysis of the two example decays have shown that the reconstruction of decays containing missing particles is possible despite the lack of information about energy and momentum. In principle these decays can be studied with the given reconstruction methods and it should be possible to put an upper bound on the branching ratios of both studied examples. For both decays upper bounds have been computed which could be achievable in an experiment with a $b\bar{b}$-cross section of 480 μb and an integrated luminosity of 1 fb^{-1}. The expected upper bounds are

$$
\begin{aligned}
\mathcal{B}(B_s^0 \to \tau^+\tau^-) &< 6.2 \times 10^{-3}, \\
\mathcal{B}(B_s^0 \to \mu^\mp\tau^\pm) &< 1.9 \times 10^{-6},
\end{aligned}
$$

both at the 95% confidence level. Due to the limited time available for this thesis it was not possible to make a complete and profound analysis. So the upper bounds

are not very reliable. Still they give a notion of what could be achievable with the presented methods.

As mentioned for the presented results there is room for improvement. So an outlook for further studies on this subject shall be given. The suggestions will be given for the different reconstruction methods separately (the BUA method will not be discussed since for the same decay topology the TDA is much more powerful):

Possible improvements for the TDA analysis method are:

- In the reconstruction of each decay the one dimensional set of solutions has been approximated with 100×100 equidistant starting points and 500×500 segments in normalized coordinates. Rising the starting point number and also the number of segments per decay will improve the resolution on the reconstructed set of solutions. However it is not clear if the better resolution in the solution space also leads to a better resolution of the physical variables such as the mass.

- For each combination in each decay the mother decay vertex candidate closest to the average mass of this combination has been selected for the reconstruction. This is a very simple way to choose a point. Storing more points or changing the selection criterion could also improve the algorithm. As an alternative selection criterion the proper time of the reconstructed daughters could be computed for each vertex candidate. Then a likelihood analysis could be done and the most probable vertex could be stored.

- In some cases the true decay vertex is located at a point where two different combinations overlap. The probability for this to happen could be studied. If it is often the case, the overlapping points could be chosen as reconstruction vertices.

- On the analysis level the analysis as such could be made separately for each combination. So far the distributions have mostly been studied for all four combinations together. Specially if the cuts are chosen for each combination separately the efficiency may rise. No specific cuts against combinatorial background have been found so far.

- The cuts that have been applied in the present analysis can certainly been approved. There are other variables that also show a good separation of signal from background. A detailed study of more cut variables could enhance the signal to background ratio. An interesting but still unused cut variable is the location of the reconstructed B_s^0 decay vertex in normalized coordinates.

Possible improvements on the TDL analysis are:

- In the TDL for each combination a single point has been chosen assuming that the true solution will be among those two points. In some cases it might be possible that there are more than only two convergence points. Storing as

much convergence points as are available could improve the method. However the effect of this will be quite small since the resolution on purely generated events is already very high.

- The separate analysis of both combinations could also enhance the reconstruction. Perhaps it is possible to cut against combinatorial background on the analysis level.

Appendix A

Calculation of the Upper Bounds

Here the calculations which are used to compute the upper bounds on the branching fractions given in Sections 4.3.5 and 4.4.4 are shown. The upper bounds are defined as the corresponding signal branching fraction which would allow a 2σ discovery of the decay at the 95% confidence level (C.L.) with a given integrated luminosity of $\mathcal{L}_{norm}$. Let N_{cut}^{bg} be the number of background events that are left after all the cuts where applied and let $\mathcal{L}_{gen}^{bg}$ be the integrated luminosity which corresponds to the generated background sample used in the analysis. Then N_{cut}^{bg} has to be normalized to $\mathcal{L}_{norm}$. The number of background events which are left for a background sample with a corresponding luminosity of $\mathcal{L}_{norm}$ is then given by $N_{norm}^{bg} = N_{cut}^{bg} \cdot \mathcal{L}_{norm}/\mathcal{L}_{gen}^{bg}$. Now let $N_{2\sigma,cut}^{sig}$ be the number of signal events which have to be left after all the cuts where applied in order to make a 2σ discovery. Using poisson statistics this number is given by the simple formula

$$N_{2\sigma,cut}^{sig} = 2 \cdot \sqrt{N_{norm}^{bg}} = 2 \cdot \sqrt{N_{cut}^{bg} \cdot \frac{\mathcal{L}_{norm}}{\mathcal{L}_{gen}^{bg}}}.$$

The situation is different when $N_{cut}^{bg} = 0$. In this case $N_{2\sigma}^{sig}$ has be computed slightly different. In order to work at the 95% C.L. the formula for $N_{2\sigma}^{sig}$ is given by

$$N_{2\sigma,cut}^{sig} = 2 \cdot 3 \cdot \sqrt{\frac{\mathcal{L}_{norm}}{\mathcal{L}_{gen}^{bg}}}.$$

Let ϵ_{sig} be the total efficiency in the analysis on signal. Then the number of events which have to be generated to reach the desired 2σ discovery is given by

$$N_{2\sigma,gen}^{sig} = \frac{N_{2\sigma,cut}^{sig}}{\epsilon_{sig}}.$$

The calculation of the branching fractions can now be done straightforward since the integrated luminosity for the signal sample and also the necessary number of

generated signal events are known. The signal branching fractions for a 2σ discovery
are given by

$$\mathcal{B}(B_s^0 \to \tau^+\tau^-)^{2\sigma} = \frac{N_{2\sigma,gen}^{sig}}{\mathcal{L}_{norm} \cdot \sigma_{prod}^{\tau\tau} \cdot \mathcal{B}(\tau \to 3\mathrm{prong})^2} \ ,$$

respectively

$$\mathcal{B}(B_s^0 \to \mu^\pm\tau^\mp)^{2\sigma} = \frac{N_{2\sigma,gen}^{sig}}{\mathcal{L}_{norm} \cdot \sigma_{prod}^{\mu\tau} \cdot \mathcal{B}(\tau \to 3\mathrm{prong})} \ ,$$

where $\sigma_{prod}^{\tau\tau}$ respectively $\sigma_{prod}^{\mu\tau}$ are the corresponding production cross sections. These
are the formulas which where applied to compute the upper bounds given in Sections
4.3.5 and 4.4.4.

Appendix B

Detailed Single Decay Properties

A short discussion of the detailed properties of a single decay shall be given here. The properties discussed concern the one-dimensional set of mother decay vertex candidates which is obtained in each event.

B.1   The four combinations

There is a one-dimensional set of possible mother decay vertices because in the equations determining this vertex the degree of freedom is one. Some further combinatorial background appears because for the reconstruction the NR is applied twice. As it is explained in section 3.3.1, there is already a two-fold ambiguity in the reconstruction of the daughter momenta. Even in an ideal situation where all the measured variables of a decay are known without errors, this ambiguities will lead to combinatorial background. For every mother decay vertex candidate, there are four reconstructed daughter momenta. These momenta can be combined in four different ways and for each such combination the discussion in Section 3.3.3 applies. Recall that the two-fold ambiguity in the NR can be understood as forward and backward scattering of the visible decay part. So the four combinations can be ordered according to the solutions which are combined. For each combination an own continuos subset of solutions can be obtained. These four subsets for a single decay are illustrated in Figure B.1. The combinations are labeled according to their interpretation:

- In the first histogram both visible parts decay forward (FF Combination).

- The second and third histogram show forward-backward decay, respectively backward-forward decay (FB Combination and BF Combination)

- The last histogram shows the combination where both visible parts decay backward (BB Combinations)

Since the different solutions correspond to different momenta of the daughter particles, the sum of the momenta at the same point is not equal for the different combinations. So mostly at each mother decay vertex candidate only one of the solutions satisfies the balancing condition of the momenta, i.e. at most one combination satisfies $\Delta p_\perp \equiv 0$[1]. So the sets of mother decay vertex candidates for the different combinations are only overlapping at four or five points. To understand this it is important to recall that for a decay angle of $\varphi = \pi/2$ the two fold ambiguity in the NR disappears. This is because then forward and backward decays are the same. The vertex candidates that balance the momenta of two combinations simultaneously are those where for one combination the restframe decay angle of the visible prong part is $\pi/2$. Only there two solutions take the same value. For each decay vertex candidate where one of the restframe decay angles is equal to $\pi/2$, there are still two solutions from the other reconstructed daughter. Since this is the case once for each daughter, four points can be found where the different combinations overlap. A fifth point is possible when the decay angles for both sides are symmetric. In this case also two of the combinations take the same value at the same place. So there are four or five points where the different combinations overlap. In total four one-dimensional subsets of possible reconstruction vertices for each event are obtained. Together these four solution form a one-dimensional set of possible decay vertices, which is mostly continuous and connected. The five overlapping points can be seen in Figure B.1.

B.2   The effect of smearing on the solutions

The one-dimensional sets which have been discussed so far, always referred to an ideal situation where all the variables are known without errors. A priori it is not clear what happens to this solution space when errors are included. In order to study the effect of smearing, the solution space of four different decays are displayed in Figures B.3 and B.2. The different decays are labeled with the event number in which they are contained. On the left hand side, the true solution space is displayed, whereas on the right hand side the solution space of the same decay is shown but now with smeared momenta and vertices. Clearly the shape of the curves are changed, but they still seem to be one-dimensional objects. There are also decays where the smearing makes a reconstruction impossible, when the NR does not provide solutions anymore. So when errors are introduced not only the distributions are broadened, but also the efficiency of the reconstruction goes down.

---

[1]for the proper definition of this value see also 3.3.3
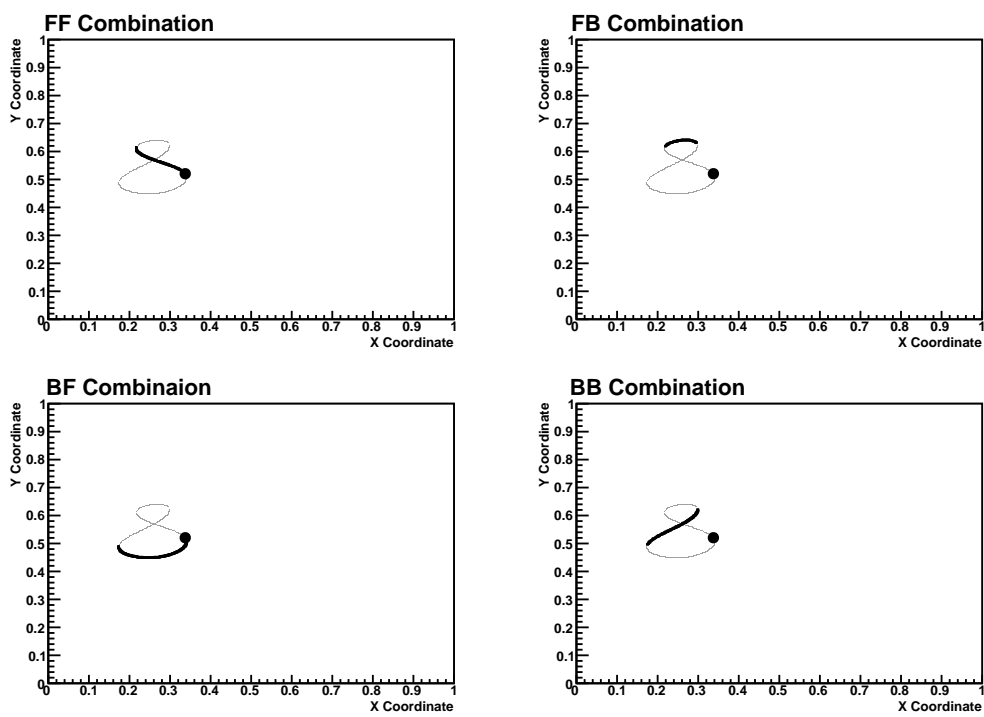
Figure B.1: The four solutions of a single event in normalized coordinates.
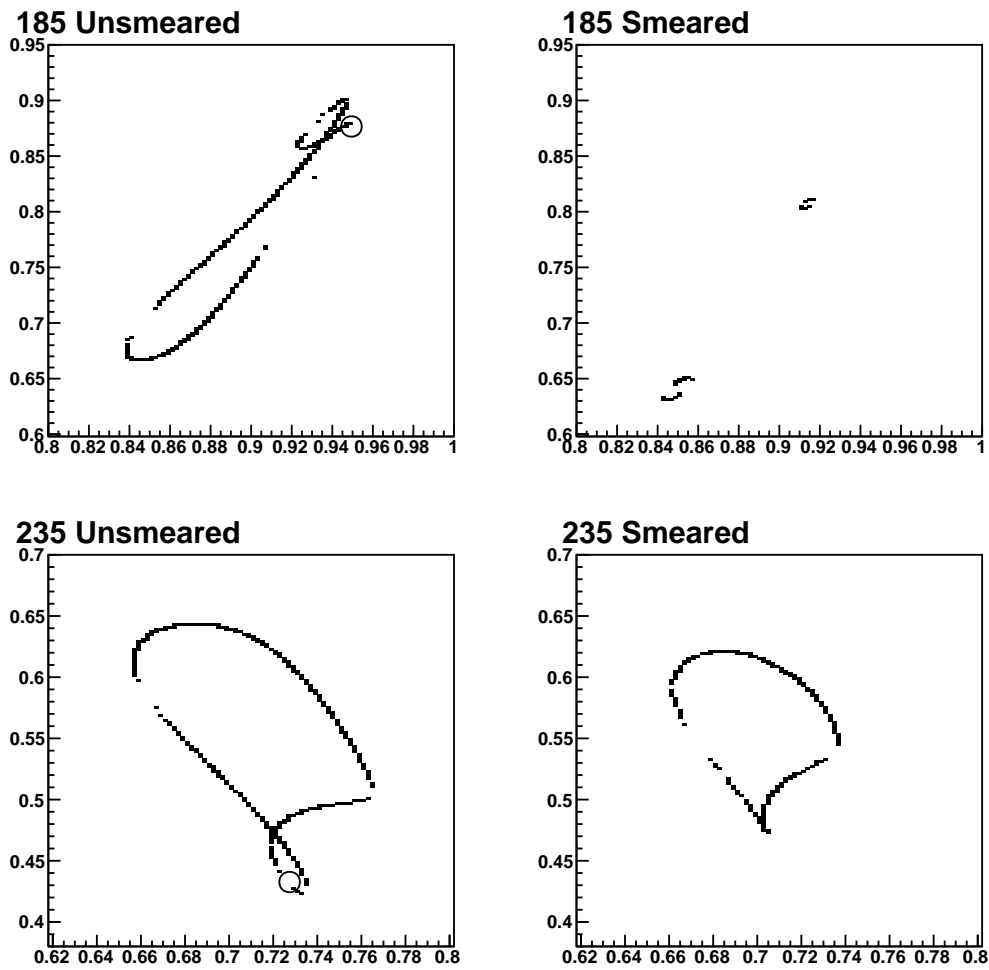
Figure B.2: The solution space of single events in normalized coordinates, once smeared and once unsmeared. The circle indicates the location of the true decay vertex. The numbers of the histograms correspond to the numbers of the event in the signal sample.

294 Unsmeared

294 Smeared

364 Unsmeared

364 Smeared
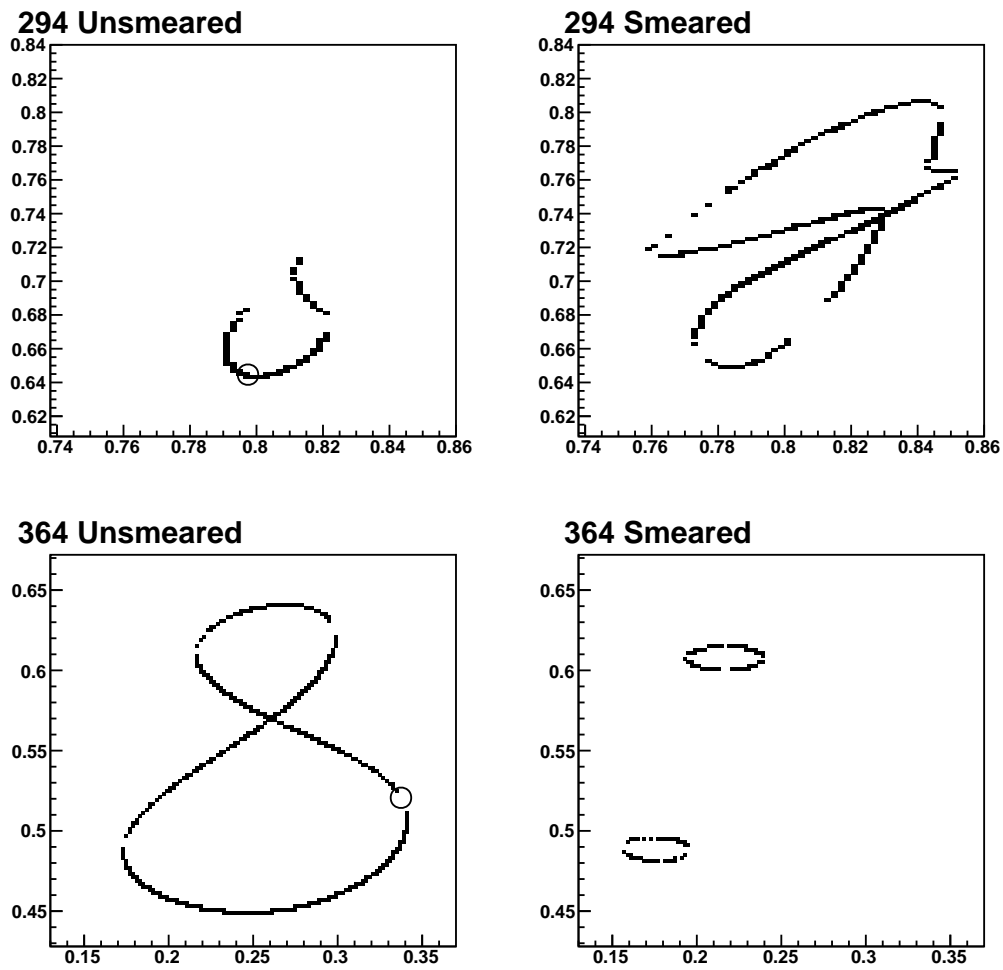
Figure B.3: The solution space of single events in normalized coordinates, once smeared and once unsmeared. The circle indicates the location of the true decay vertex. The numbers of the histograms correspond to the numbers of the event in the signal sample.

Appendix C

Histograms on $B_s^0 \rightarrow \tau\tau$

There are many possible variables which could be interesting to understand the kinematics of a decay. The non-trivial decay topology allows the reconstruction of many variables for each event. In the main body of this work only the most relevant and interesting distributions are presented. Here also some distributions of other variables are shown. All the plots are shown twice, once the histograms are shown for signal and generic background and once the histograms are shown for signal and resonant background. In both cases the histograms are as far as possible grouped according to the following criteria (the numbers of the figures indicate generic/resonant background):

- In Figures C.1/ C.5 the kinematical properties of the particles are shown (pseudo-rapidity η and $p_\perp$).

- In Figures C.2/C.6 the angles between the vertices and their length are shown

- In Figures C.3/C.7 some angles between the momenta and the vertices are shown.

- In Figures C.4/C.8 some more variables are displayed: the position of the reconstructed B_s^0 vertex in normalized coordinates, the logarithm of the minimization value $|\Delta p_\perp|$, the 3-prong multiplicity and the reconstructed mass.

In all 1D histograms the full line displays the distribution for the signal sample whereas the dashed line displays the generic respectively the resonant background sample. All the 1D histograms are normalized to one.
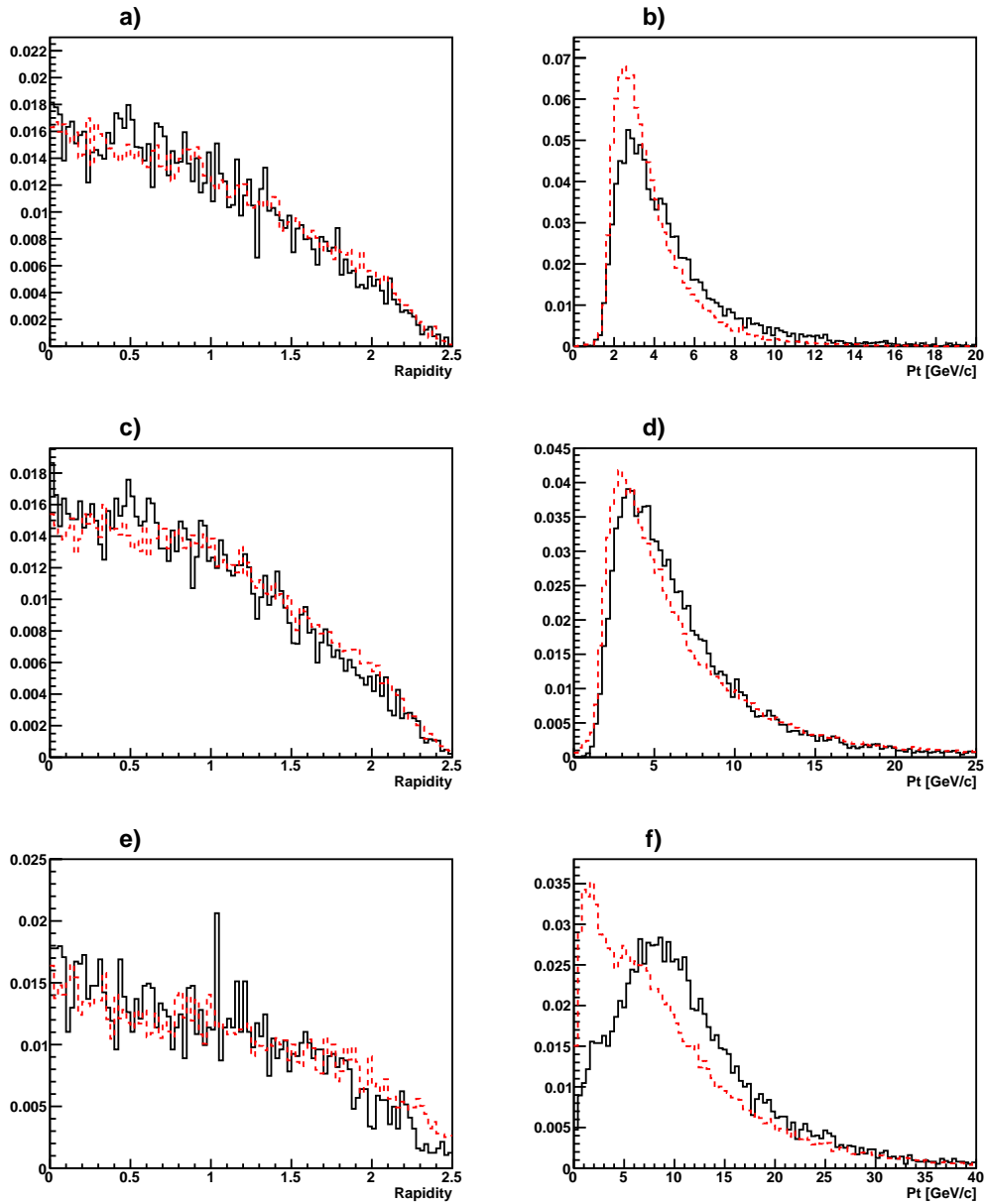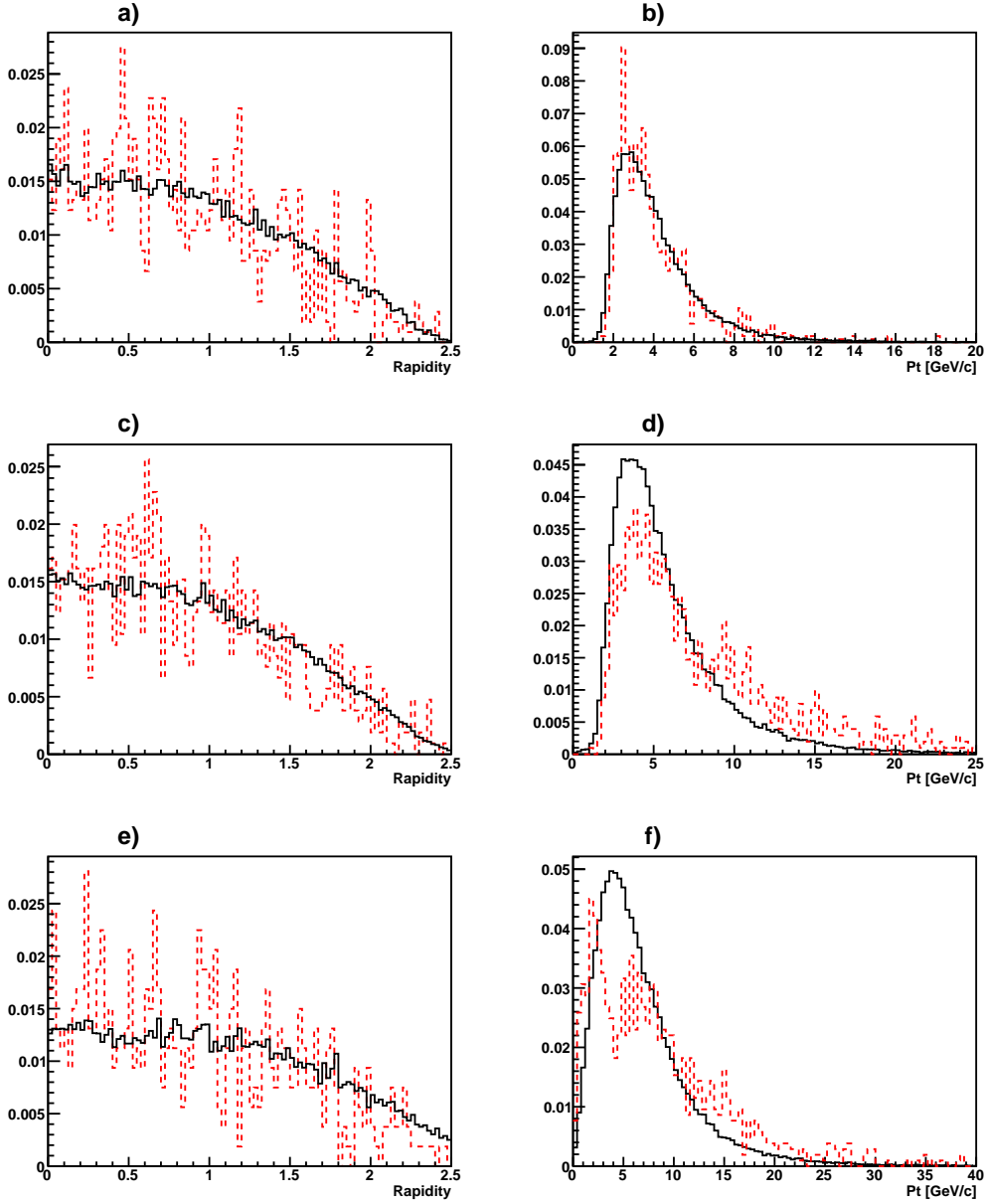
Figure C.1: Signal (full) and generic background (dashed):
The pseudo-rapidity is shown in a) for the 3-prongs, in c) for the τ-leptons and in
e) for the B_s. The distributions of the transverse momenta are shown in b) for the
3-prongs, in d) for the τ-leptons and in f) for the B_s.
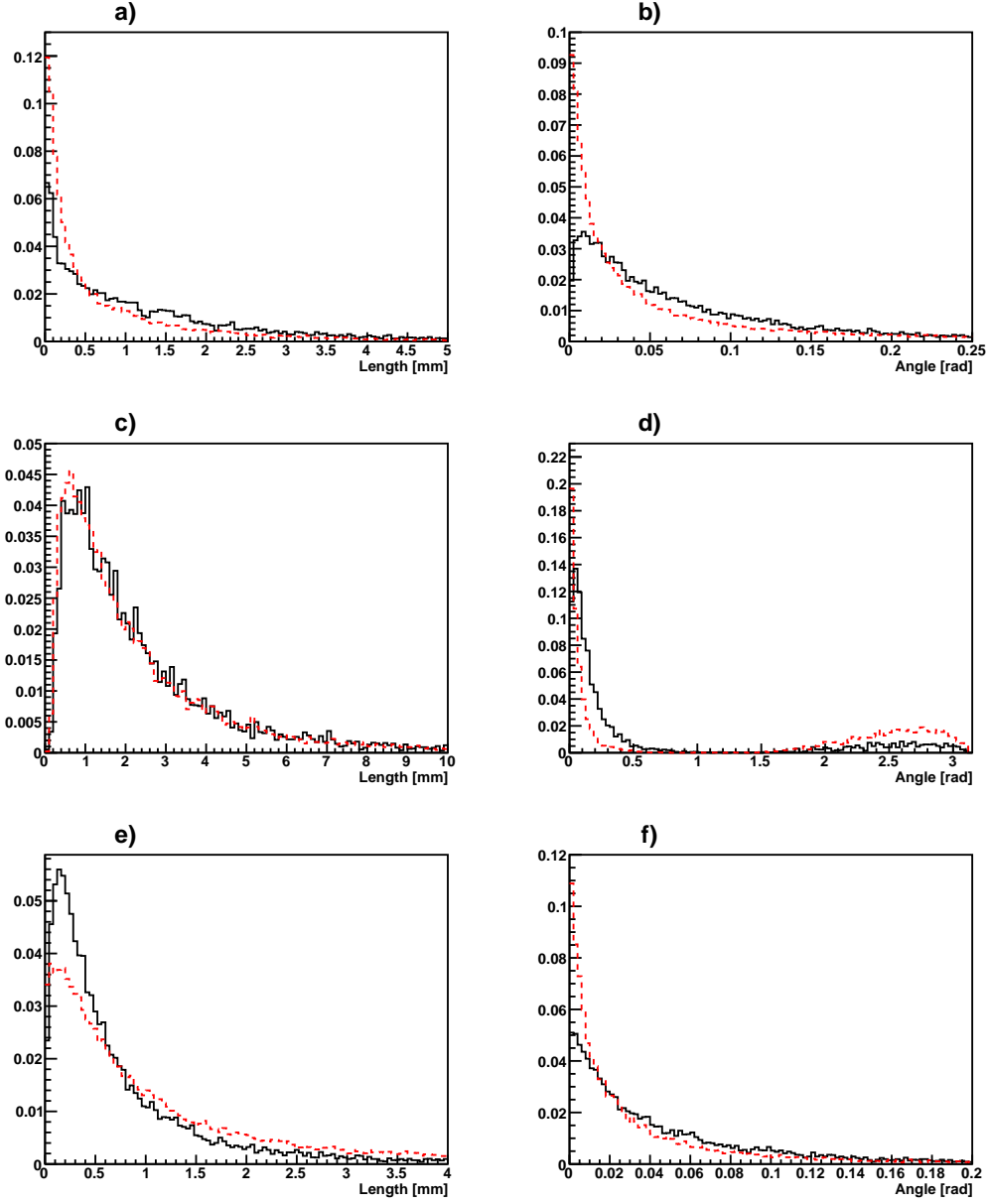
Figure C.2: Signal (full) and generic background (dashed):
a) length of the B_s^0-decay vertex, c) length of the τ-decay vertex, e) the difference between the length of the B_s^0-decay vertex and the length of the τ-decay vertex, b) angles between the B_s^0-decay vertex and the τ-decay vertices, d) the angle between the two τ-decay vertices, f) the difference between the angle shown in b) and the angle shown in d).
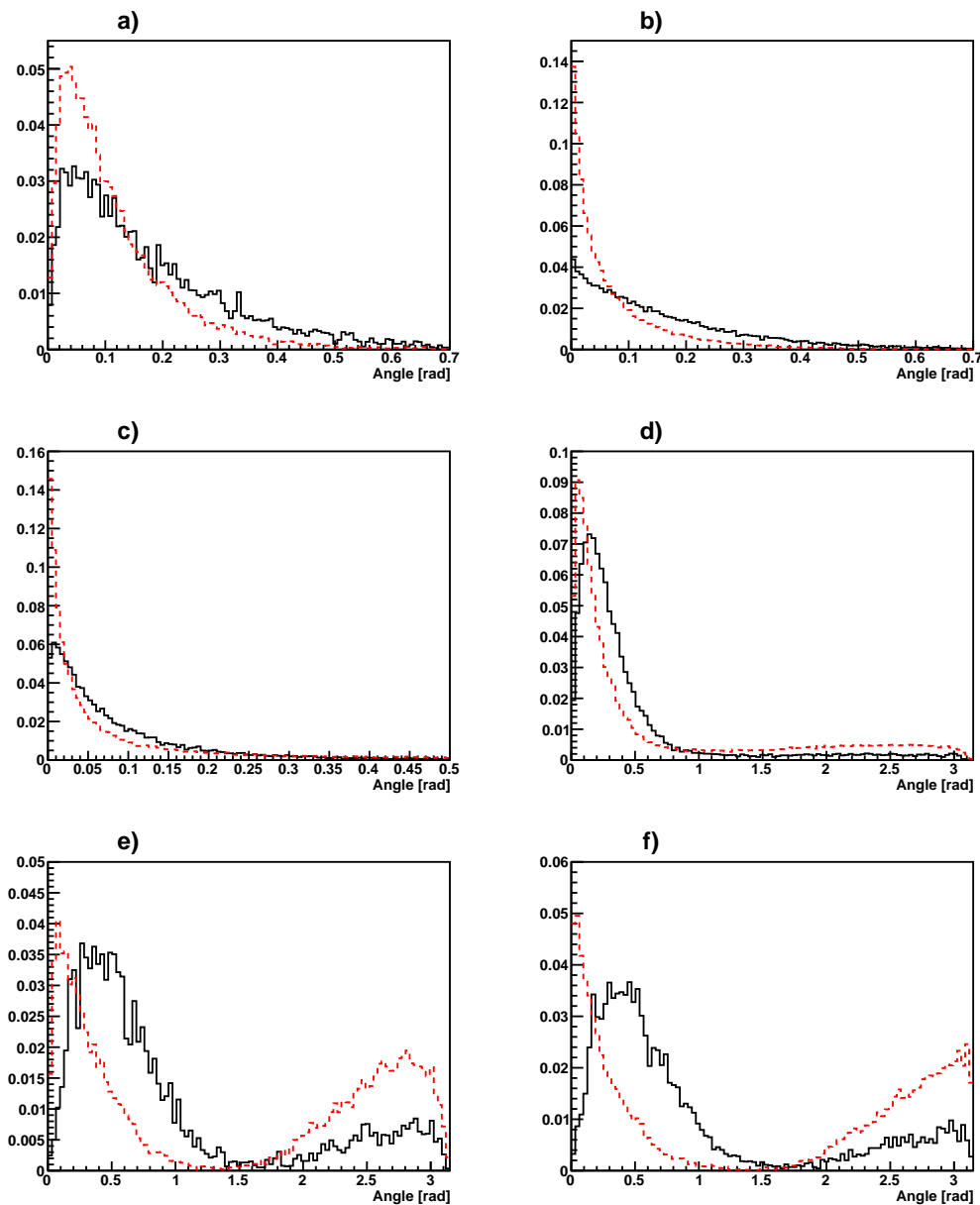
Figure C.3: Signal (full) and generic background (dashed):
a) Angle between the 3-prong momenta and the corresponding vertices, b) angle between the τ-momenta and the corresponding vertices, c) angle between the B_s^0-momentum and the τ-decay vertices, d) angle between the B_s^0-momentum and the 3-prong momenta, e) angle between the prong momenta, f) angle between the τ-momenta.
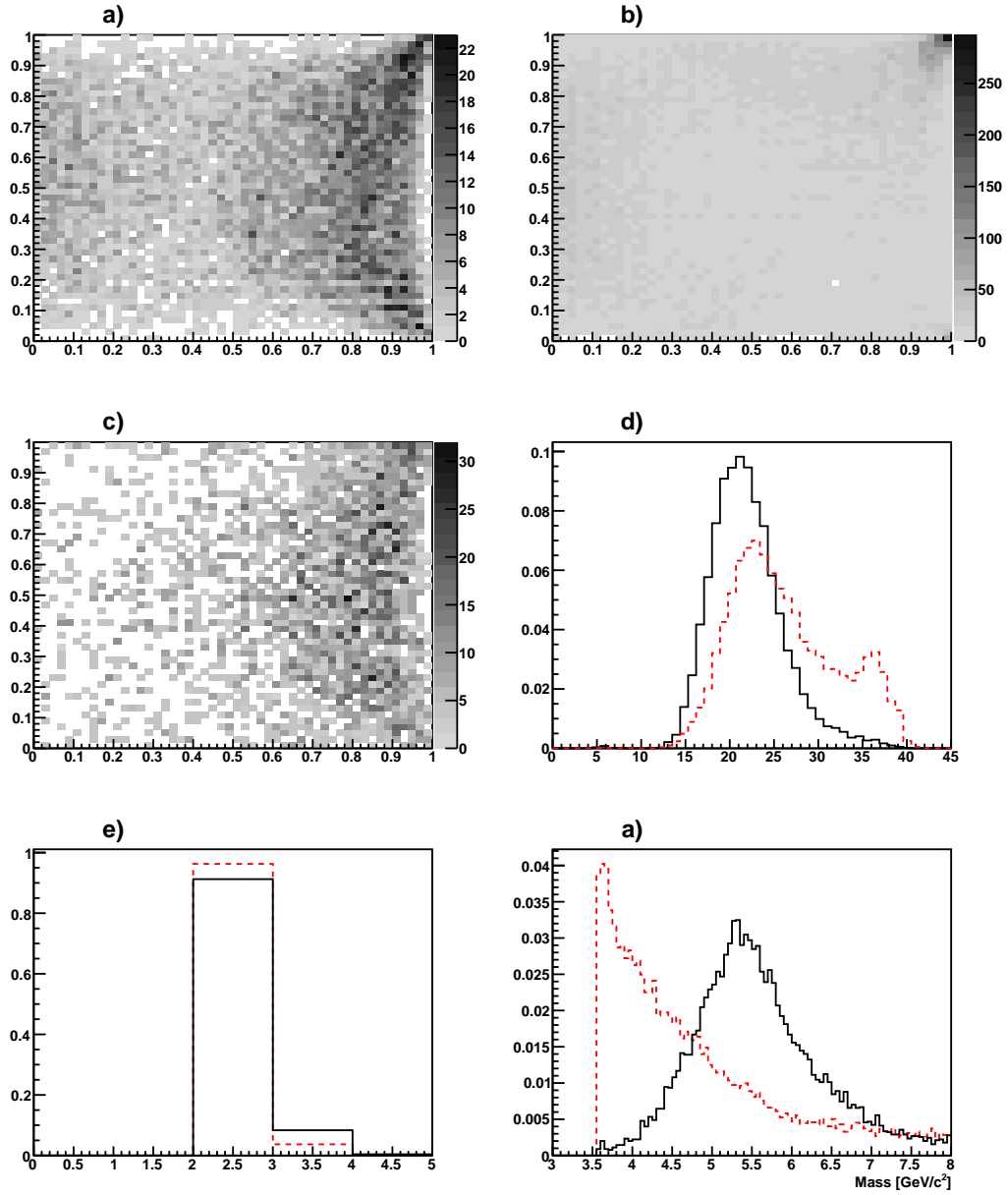
Figure C.4: Signal (full) and generic background (dashed):
The location of the reconstructed τ-decay vertices in normalized coordinates are shown in a) for signal, in b) for generic background, c) shows the true distribution for the same variable, d) shows the minimization value $-\log(\Delta p_\perp)$, e) shows the 3-prong multiplicity, f) the distribution of the reconstructed mass.
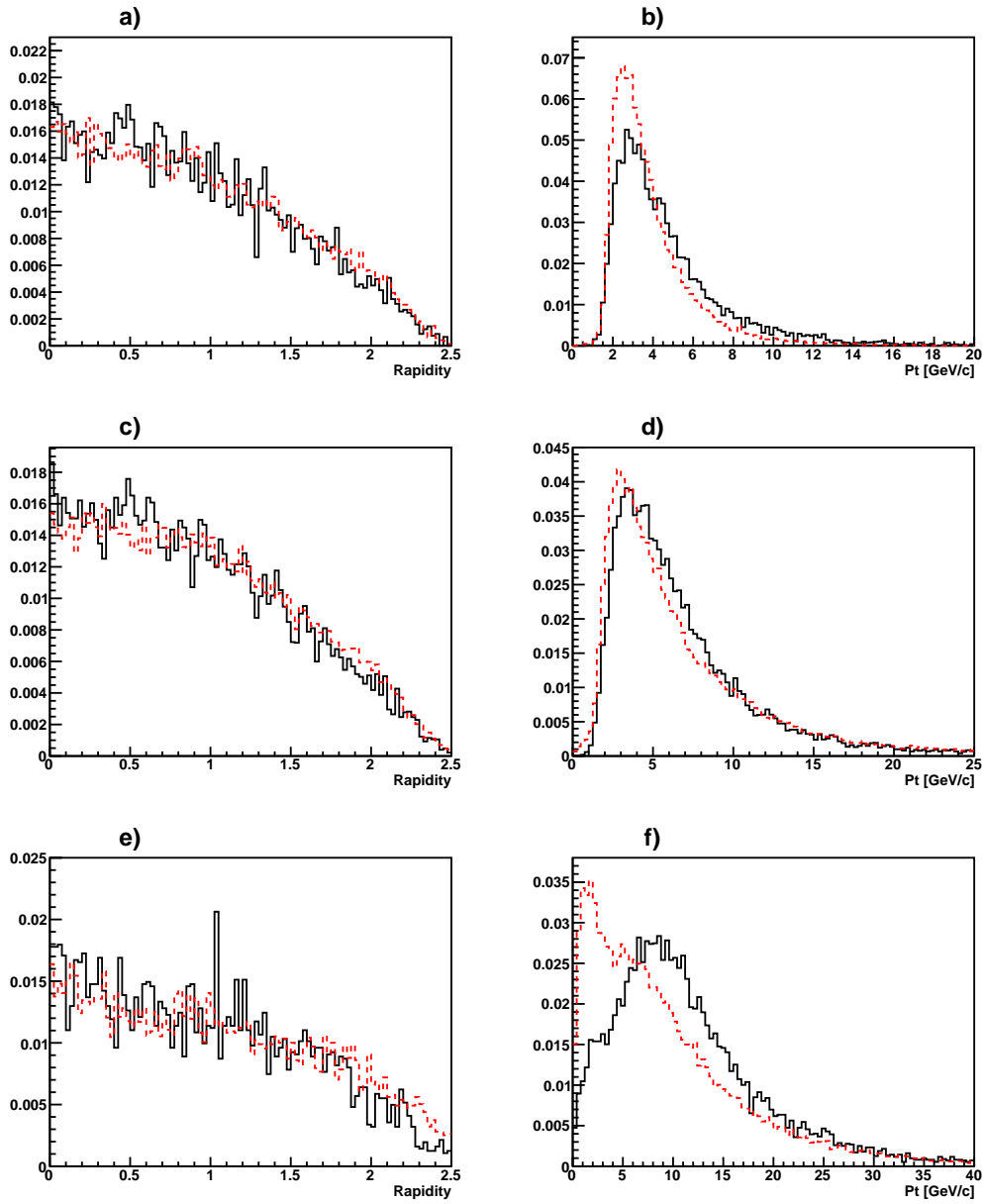
Figure C.5: Signal (full) and resonant background (dashed):
The pseudo-rapidity is shown in a) for the 3-prongs, in c) for the τ-leptons and in e) for the B_s. The distributions of the transverse momenta are shown in b) for the 3-prongs, in d) for the τ-leptons and in f) for the B_s.
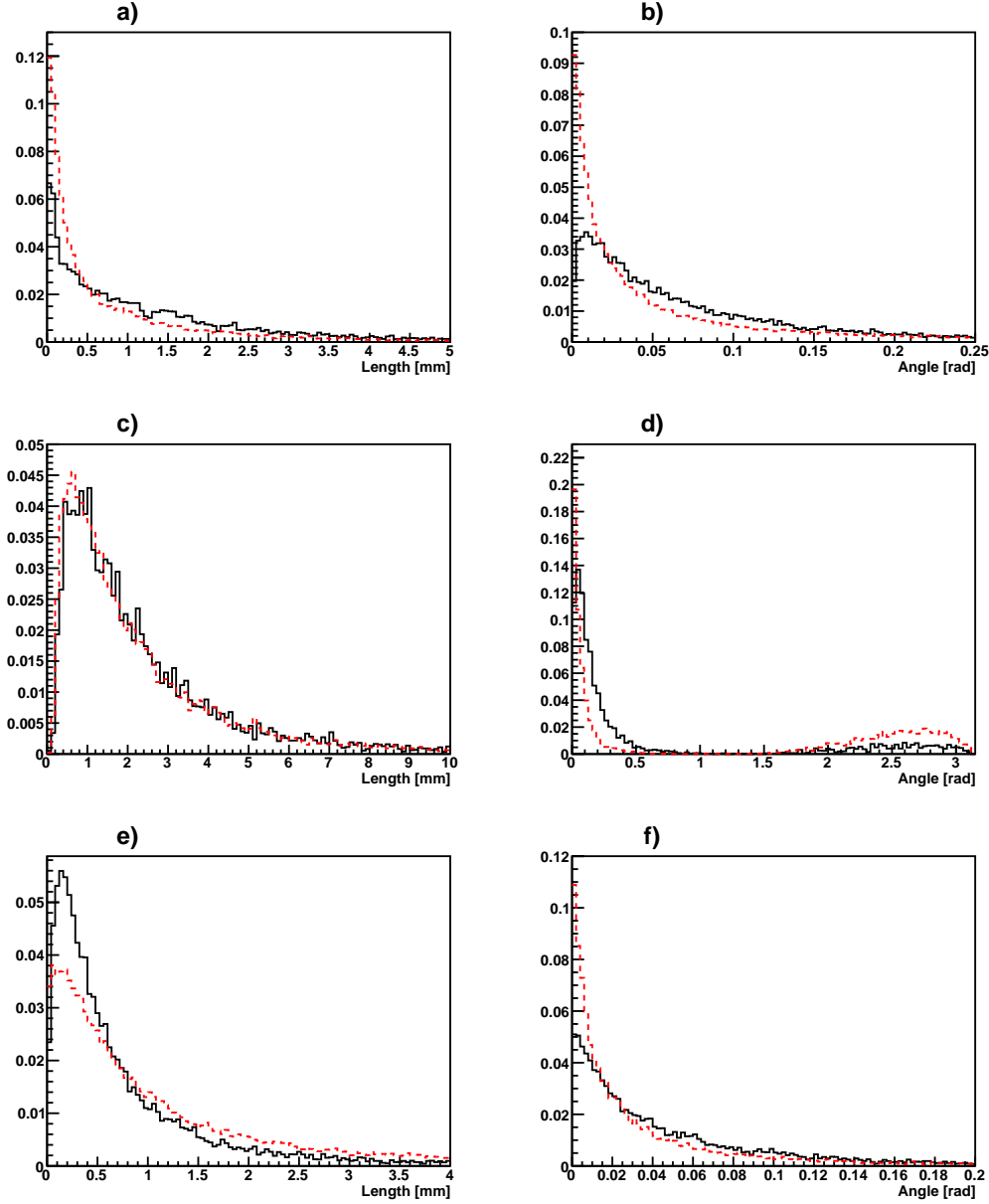
Figure C.6: Signal (full) and resonant background (dashed):
a) length of the B_s^0-decay vertex, c) length of the τ-decay vertex, e) the difference
between the length of the B_s^0-decay vertex and the length of the τ-decay vertex, b)
angles between the B_s^0-decay vertex and the τ-decay vertices, d) the angle between
the two τ-decay vertices, f) the difference between the angle shown in b) and the
angle shown in d).
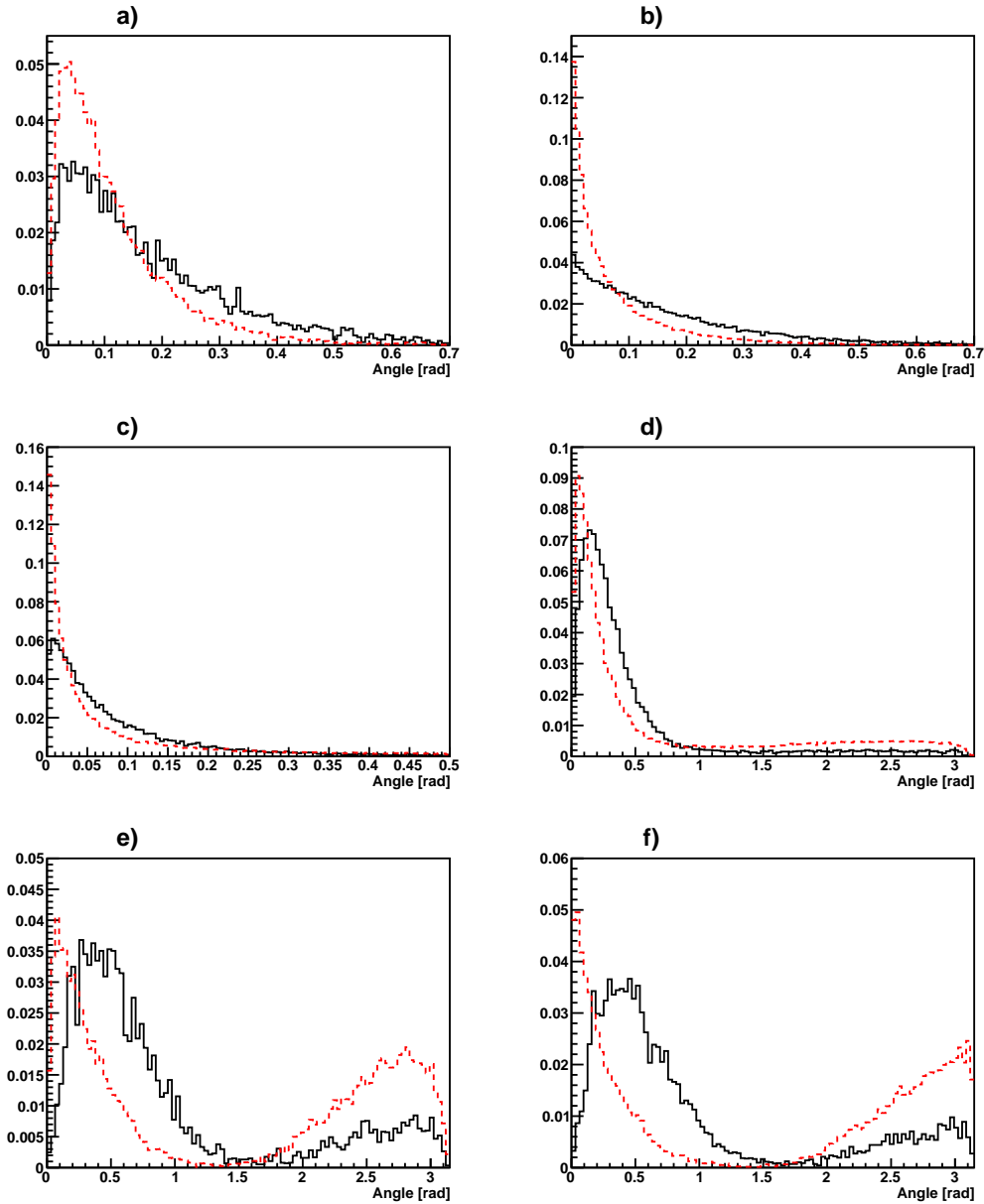
Figure C.7: Signal (full) and resonant background (dashed):
a) Angle between the 3-prong momenta and the corresponding vertices, b) angle between the τ-momenta and the corresponding vertices, c) angle between the B_s^0-momentum and the τ-decay vertices, d) angle between the B_s^0-momentum and the 3-prong momenta, e) angle between the prong momenta, f) angle between the τ-momenta.
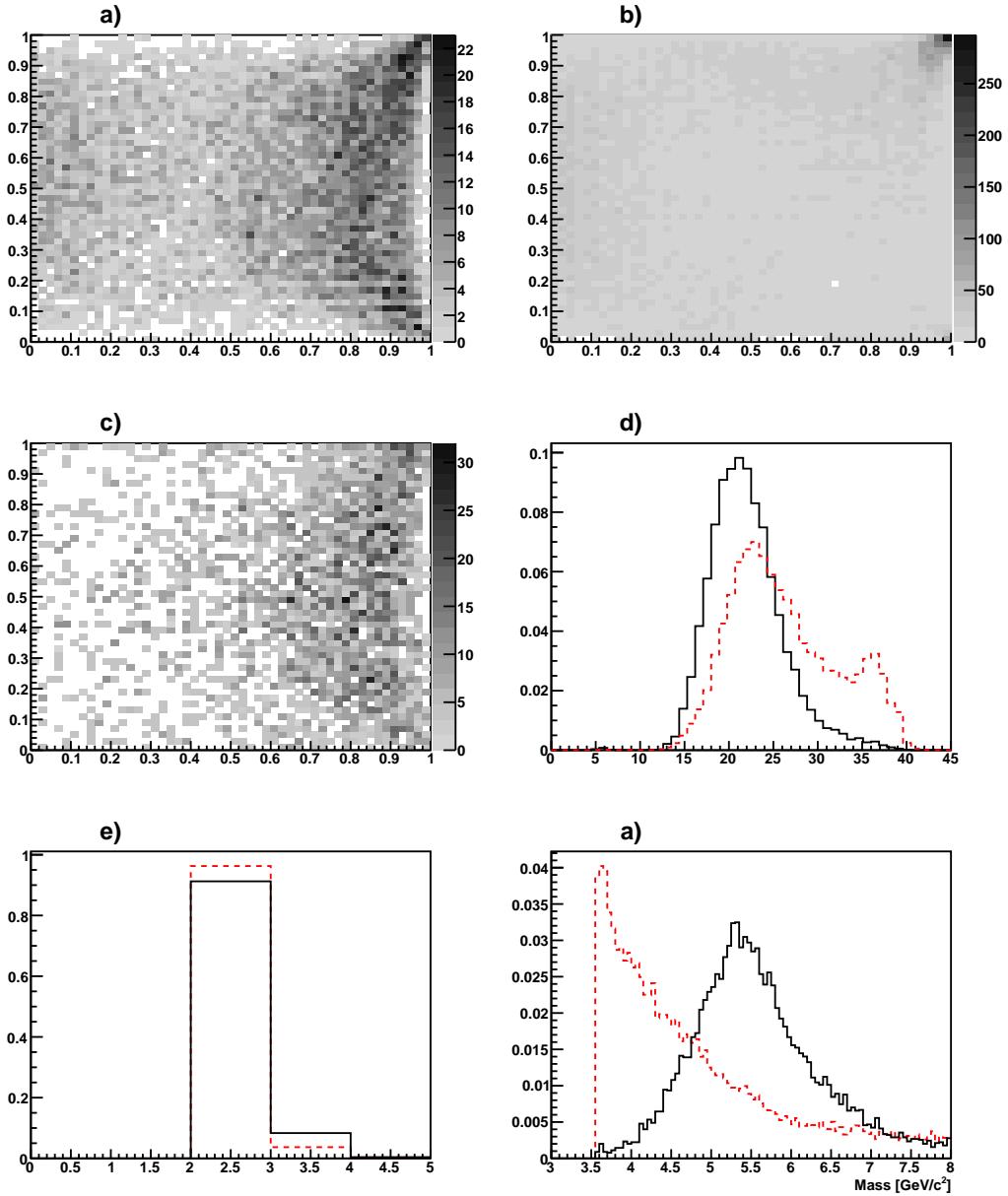
Figure C.8: Signal (full) and resonant background (dashed):
The location of the reconstructed τ-decay vertices in normalized coordinates are
shown in a) for signal, in b) for resonant background, c) shows the true distribution
for the same variable, d) shows the minimization value $-\log(\Delta p_\perp)$, e) shows the
3-prong multiplicity, f) the distribution of the reconstructed mass.

Appendix D

Histograms on $B_s^0 \rightarrow \mu^\pm \tau^\mp$

The histograms for this decay are similar to the $B_s \rightarrow \tau\tau$ decay. A difference is the muon appearing in each event. The muon provides some more histograms. Again the histograms are as far as possible ordered according to the following criteria:

- In Figure D.1 the rapidity and the transverse momentum on the 3-prong, the tau and the B_s are shown.

- In Figure D.2 the geometrical properties of the vertices and the impact parameter are shown.

- In Figure D.3 the angles between the momenta and the vertices respectively the impact factor are shown.

- In Figure D.4 the properties of the muon of each decay are shown.

- In Figure D.5 some more variables are displayed: the coordinate along the muon track indicating the reconstructed B_s decay vertex (the position zero is at the impact parameter), the minimization variable (i.e. the momentum balance), the reconstructed mass (before cuts and unweighed), the 3-prong multiplicity and the muon multiplicity.

In all histograms the full line displays the distribution for the signal sample whereas the dashed line displays the generic background sample. All histograms are normalized to one.

Figure D.1: The pseudo-rapidity is shown in a) for the 3-prong, in c) for the τ-lepton and in e) for the B_s. The distributions of the transverse momenta are shown in b) for the 3-prongs, in d) for the τ-lepton and in f) for the B_s.
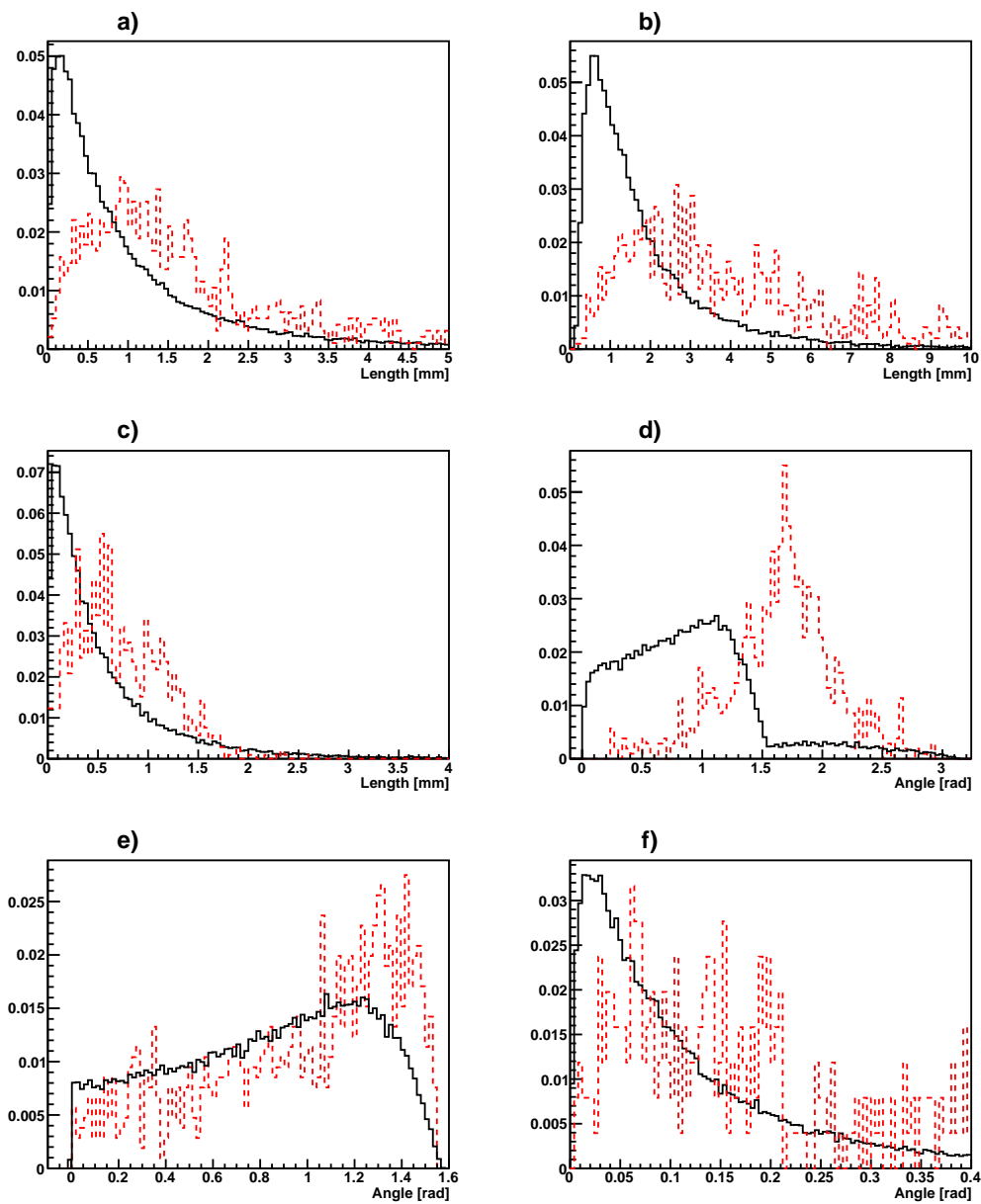
Figure D.2: a) length of the B_s^0-decay vertex, b) length of the τ-decay vertex, c) length of the impact parameter, d) angle between the impact parameter and the τ-decay vertex, e) angle between the impact parameter and the B_s^0-decay vertex, f) angle between the B_s^0-decay vertex and the τ-decay vertex.
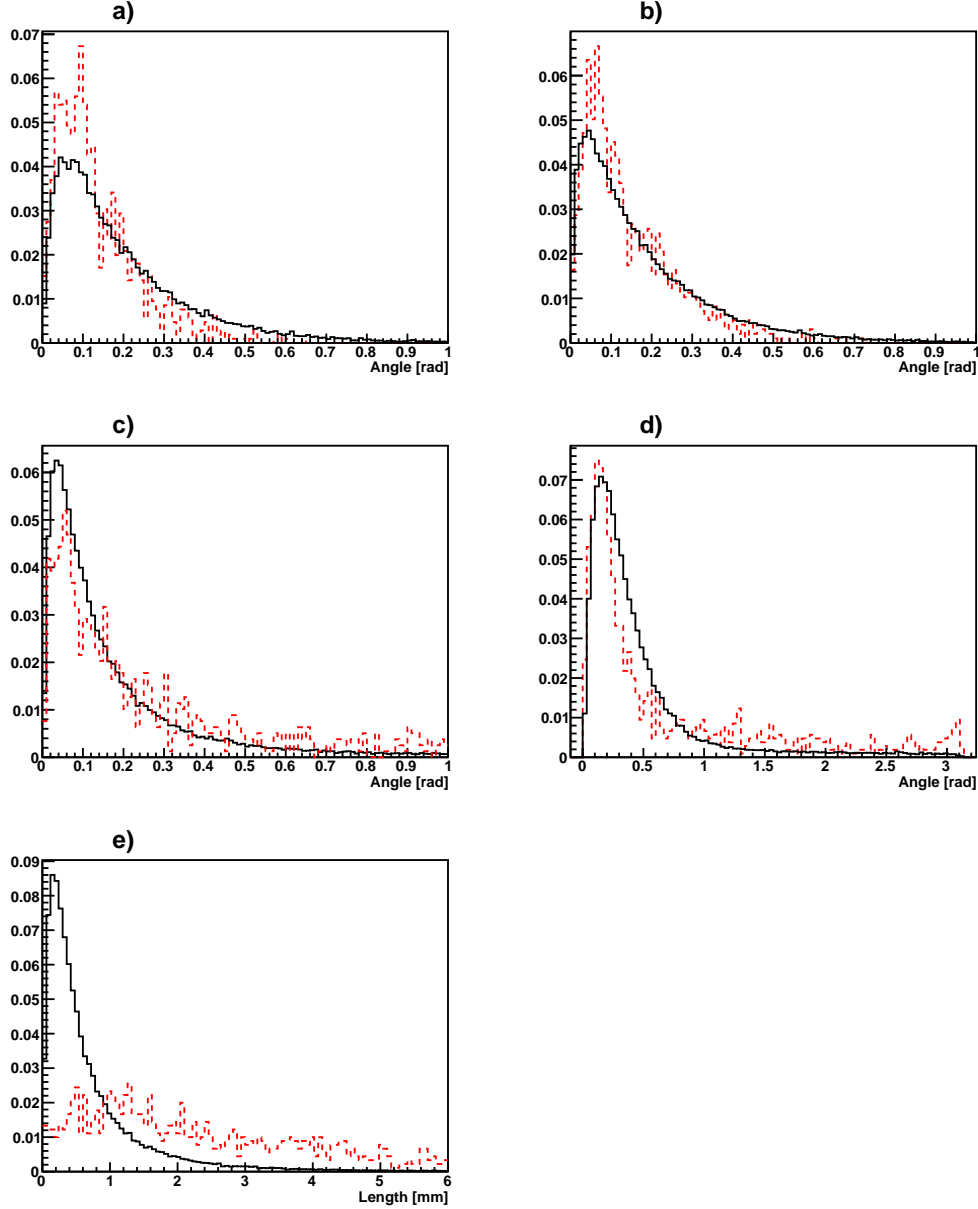
Figure D.3: a) Angle between the 3-prong momentum and the τ-decay vertex, b) angle between the τ-momentum and the τ-decay vertex, c) angle between the B_s^0-momentum and the τ-decay vertex, d) angle between the B_s^0-momentum and the 3-prong momentum, e) the difference between the length of the B_s^0-decay vertex and the length of the τ-decay vertex.
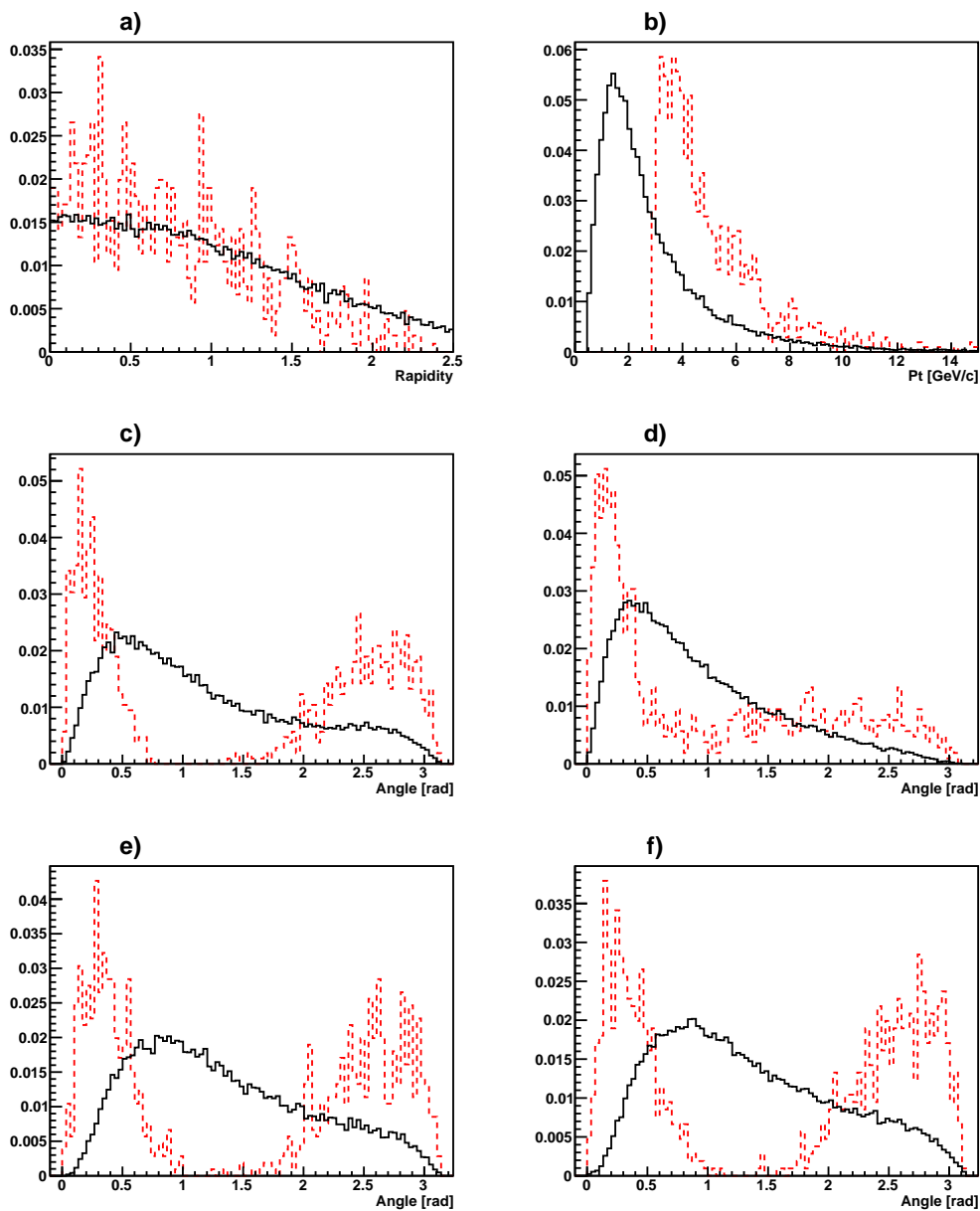
Figure D.4: a) rapidity of the μ-lepton, b) transverse momentum of the μ-lepton, c) angle between the momentum of the μ-lepton and the τ-decay vertex, d) angle between the B_s^0-momentum and the momentum of the μ-lepton, e) angle between the 3-prong momentum and the momentum of the μ-lepton, f) angle between the τ-momentum and the momentum of the μ-lepton.
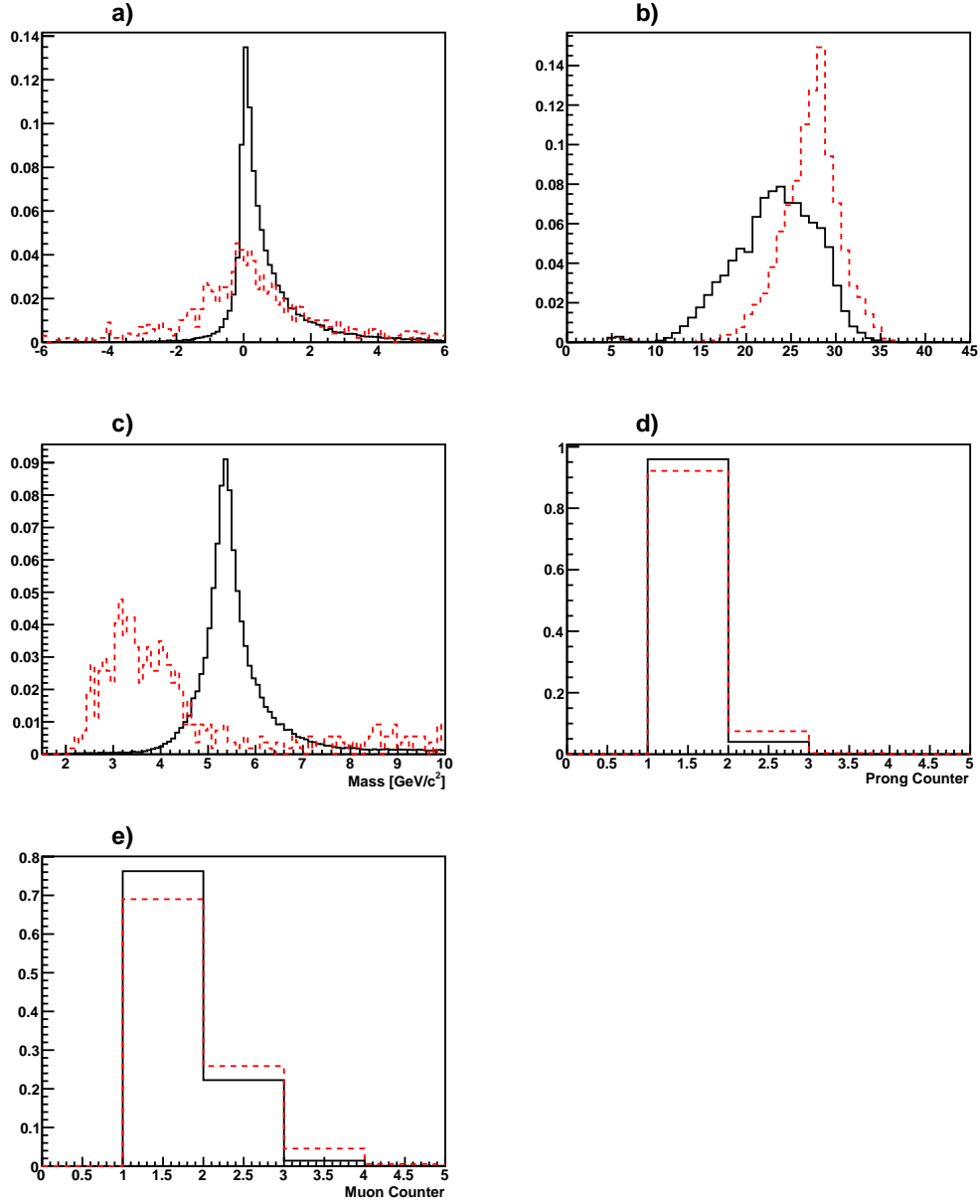
Figure D.5: a) location of the reconstructed B_s^0-decay vertex along the muon track measured from the impact parameter, b) minimization value $-\log(\Delta p_\perp)$, c) the distribution of the reconstructed mass, d) 3-prong multiplicity, e) muon multiplicity.

Acknowledgements

List of Figures

List of Tables

Bibliography

[1] B. Aubert *et al.* [BABAR Collaboration], Phys. Rev. Lett. **96** (2006) 241802 [arXiv:hep-ex/0511015].

[2] A. Abulencia *et al.* [CDF Collaboration], Phys. Rev. Lett. **95** (2005) 221805 [Erratum-ibid. **95** (2005) 249905] [arXiv:hep-ex/0508036].

[3] J. P. Saha and A. Kundu, Phys. Rev. D **66** (2002) 054021 [arXiv:hep-ph/0205046].

[4] R. Van Kooten, *In the Proceedings of 4th Flavor Physics and CP Violation Conference (FPCP 2006), Vancouver, British Columbia, Canada, 9-12 Apr 2006, pp 031* [arXiv:hep-ex/0606005].

[5] J. E. Duboscq, Nucl. Phys. Proc. Suppl. **144** (2005) 265 [arXiv:hep-ex/0412022].

[6] A. Dedes, J. R. Ellis and M. Raidal, Phys. Lett. B **549** (2002) 159 [arXiv:hep-ph/0209207].

[7] S. Dambach, U. Langenegger and A. Starodumov, Nucl. Instrum. Meth. A **569**, 824 (2006) [arXiv:hep-ph/0607294].

[8] A. J. Buras, Phys. Lett. B **566** (2003) 115 [arXiv:hep-ph/0303060].

[9] G. Isidori, AIP Conf. Proc. **722**, 181 (2004) [arXiv:hep-ph/0401079].

[10] W. Skiba and J. Kalinowski, Nucl. Phys. B **404** (1993) 3.

[11] J. Kalinowski, arXiv:hep-ph/0309235.

[12] L. Randall and R. Sundrum, Phys. Rev. Lett. **83** (1999) 3370 [arXiv:hep-ph/9905221].

[13] G. Bertone, D. Hooper and J. Silk, Phys. Rept. **405** (2005) 279 [arXiv:hep-ph/0404175].

[14] B. Koch, M. Bleicher and S. Hossenfelder, JHEP **0510** (2005) 053 [arXiv:hep-ph/0507138].

[15] W.-M. Yao *et al.*, Journal of Physics G 33, 1 (2006)

[16] DMK/DPK, Formeln und Tafeln, 7. Auflage (1997)